



universität
wien

DIPLOMARBEIT

Titel der Diplomarbeit

A Mathematical Model of Actin-Myosin Interaction and its Application to Keratocyte Movement

angestrebter akademischer Grad

Magistra der Naturwissenschaften (Mag rer. nat.)

Verfasserin: Angelika Manhart
Matrikel-Nummer: A 0405785
Studienrichtung: A 405 Mathematik
Betreuer: Univ.-Prof. Dr. Christian Schmeiser

Wien, Mai 2011

Contents

Acknowledgements	iii
Abstract	v
German Summary - Deutsche Zusammenfassung	vii
1 Introduction and Biological Background	1
1.1 Laboratory Work	1
1.2 Mobility and the Cytoskeleton	1
1.3 Actin	4
1.4 Myosin	5
1.5 Interaction in Muscles	6
1.6 Lamellipodium	8
1.7 Basic Vocabulary	9
2 Modeling of Actin-Myosin Interaction	11
2.1 Derivation of the Model	11
2.2 Analysis of ODE Moment System	13
2.3 Stationary Equation	15
2.3.1 The Characteristics	16
2.3.2 Calculating the Stationary Solution	18
2.4 Full Equation	20
2.4.1 Calculating the Full Solution	20
2.4.2 Longtime Behavior	22
2.5 Interpretation	25
2.6 Appendix	26
2.6.1 Where to define Initial Conditions	26
2.6.2 Properties of the Matrix Exponential	29
3 Application to Keratocyte Movement	31
3.1 Introduction	31
3.2 Lamellipodium Modeling	32
3.2.1 Assumptions and General Modeling	32
3.2.2 The Limit of instantaneous Cross Link and Adhesion Turnover	36
3.3 Introducing Myosin to the Model	40
3.3.1 Observations and Modeling	40
3.3.2 Deriving Energy Contributions	41
3.3.3 Non-dimensionalization and Scaling the Energy Contributions	42
3.3.4 Modeling the Dependencies on the Size of a Myosin Filament	45
3.4 Outlook	48
Bibliography	i
Curriculum Vitae	iii

Acknowledgements

First of all I would like to thank my supervisor Christian Schmeiser, whose encouragement and guidance enabled me to get a deeper understanding of the subject. I also want to express my gratitude to Vic Small and Nikolaos Sfakianakis for their support and help. Further I want to thank Steffi, Florian and my roommates Marina and Alena for all the helpful advice, long discussions and also for being there in working breaks when I needed to clear my head.

Lastly, this diploma thesis would not have been possible without the support of my parents throughout my studies, who showed great patience in enduring my partly chaotic working habits and also helped with proofreading. Special thanks to my father for going with me through some calculations and proofs, which helped me ordering my thoughts.

Abstract

This work aims at a better understanding of processes, which form the basis of cell movement. This movement plays an important role in a variety of very different situations; without them most forms of life would be unthinkable.

The basis for cellular movement is in many cases the filament-forming protein actin, which can be found in all eukaryotic cells. The focus lies on the interaction between actin and the motor protein myosin. Myosin can also form filaments, but in contrast to actin, they are symmetric and have many small "heads". These have the ability to move under consumption of energy along actin, or drag actin into a direction. This is for example the case in our skeletal muscles and no matter if we move our fingers to turn a page or take part in a marathon, actin-myosin interactions are responsible.

After an introduction to the biological basics in Chapter 1, a detailed mathematical model for the interactions is derived in Chapter 2. The modeling tries to take into account all essential forces which act on attached myosin heads. It leads to a non-linear kinetic transport equation for a distribution function Ψ , which describes the number of bound myosin heads in dependence of their position and velocity. Two things are unusual about this equation: First the usage of Delta distributions which only put heads on very specific positions with very specific speed. And secondly, it is possible to derive a system of closed ordinary differential equations for the moments of Ψ , i.e. the total number of attached heads, the average myosin bundle speed and the total stress. It can be shown that their (unique) steady states are globally stable.

After solving the moment system, the transport equation can be solved by the methods of characteristics. It turns out that the influence of a given initial distribution decays with time and that the remaining part is concentrated on a single curve in phase space. Responsible for this effect are the deltas in the equation. For $t \rightarrow \infty$ the solution converges to a stationary solution.

Finally in Chapter 3 the considerations about actin-myosin interactions are applied to the concrete situation of keratocytes (motile fish cells). These cells have a thin, sheet-like protrusion, called lamellipodium, in which many actin filaments can be found. They are used for the movement of the cells and form a network, in which the filaments are connected to each other and the substrate. Keratocytes are either stationary and circular shaped or half-moon shaped and moving. The consequences of actin-myosin interactions are added to an existing model about the movement of keratocytes. The model starts with a discrete description, then lets the number of filaments tend to infinity and derives for each effect an energy functional, which the filament positions seek to minimize. The idea is that myosin can help destabilizing the stationary state and lead to a transition to the moving state. For myosin we assume the ability to walk towards one end of actin and to move the angle between two actin filaments towards 180 degrees. Myosin filaments can grow and the created forces are assumed to be dependent on this size. Looking at the variational problem leads to an Euler-Lagrange equation. The next step to be done would be an implementation of the myosin terms into an existing Matlab code to check that the keratocyte's stationary state can be destabilized and transformed to a moving state.

German Summary - Deutsche Zusammenfassung

Zielsetzung dieser Diplomarbeit ist das bessere Verständnis von Prozessen, die der eigenständigen Bewegung von Zellen zugrunde liegen. Zellbewegungen spielen in einer großen Anzahl sehr unterschiedlicher Situationen eine wesentliche Rolle; ohne sie wären die meisten Formen von Leben nicht denkbar.

Basis für Zellbewegung ist in vielen Fällen das filament-bildende Protein Aktin, welches in allen eukaryoten Zellen zu finden ist. Der Fokus dieser Arbeit liegt auf dem Zusammenspiel zwischen Aktin und dem Motorprotein Myosin. Auch Myosin kann Filamente bilden, welche, im Unterschied zu Aktin, symmetrisch sind und viele kleine "Köpfe" besitzen. Diese haben die Fähigkeit unter Energieverbrauch auf Aktin entlang zu wandern, beziehungsweise Aktin in eine Richtung zu ziehen. Das ist etwa in allen unseren Skelettmuskeln in einer sehr organisierten Form der Fall und egal ob wir die Finger bewegen, um eine Seite umzublättern oder an einem Hürdenlauf teilnehmen, Aktin-Myosin Wechselwirkung sind dafür verantwortlich.

Nach einer Einführung in die molekularbiologischen Grundlagen in Kapitel 1 wird in Kapitel 2 ein detailliertes mathematisches Model für die Wechselwirkungen zwischen Aktin und Myosin hergeleitet. Die Modellierung versucht die wesentlichen physikalischen Kräfte zu beschreiben, die auf einen Myosinkopf wirken und führt auf eine nicht-lineare kinetische Transportgleichung für eine Verteilungsfunktion Ψ , welche die Anzahl der gebundenen Köpfe in Abhängigkeit ihrer Position und Geschwindigkeit beschreibt. Ungewöhnlich an dieser Gleichung ist einerseits die Verwendung von Delta-Distributionen, die neu gebundene Köpfe nur an ganz bestimmte Positionen mit ganz bestimmten Geschwindigkeiten setzen. Die zweite Besonderheit ist die Tatsache, dass sich für die Momente der Verteilungsfunktion, d.h. für die Anzahl der gebundenen Köpfe, die Geschwindigkeit des Myosinbündels und die Gesamtbelastung ein geschlossenes, autonomes System nicht-linearer, gewöhnlicher Differenzialgleichungen ergibt. Eine Stabilitätsanalyse des Ode-Systems zeigt, dass die (eindeutigen) Gleichgewichtspunkte global stabil sind.

Nachdem das Moment-System gelöst ist, kann die Transportgleichung durch die Charakteristiken-Methode gelöst werden. Es zeigt sich, dass der Einfluss einer vorgegebenen Anfangsverteilung mit der Zeit abnimmt und der restliche Anteil zu jedem Zeitpunkt auf einer einzelnen Kurve konzentriert ist; dafür verantwortlich sind die Deltas in der Gleichung. Im Limes konvergiert die Lösung gegen eine stationäre Lösung.

In Kapitel 3 schließlich wird versucht die Überlegungen der Aktin-Myosin Interaktionen auf die konkrete Situation von Keratozyten (bewegliche Fischzellen) anzuwenden. Diese Zellen besitzen einen dünnen, blattartigen Fortsatz, welcher Lamellipodium genannt wird und zahlreiche Aktinfilamente enthält, welche zur Fortbewegung verwendet werden. Diese Filamente bilden ein Netzwerk, in welchem die Filamente untereinander und mit der Oberfläche verbunden sind. Keratozyten befinden sich entweder in einem runden, stationären Zustand oder in einem halbmondförmigen, beweglichen Zustand. Einem bestehenden Modell zur Bewegung von Keratozyten (Oelz and Schmeiser [2010c]) werden die Auswirkungen von Aktin-Myosin Interaktionen hinzugefügt. Das Modell beginnt mit einer diskreten Beschreibung, lässt anschließend die Anzahl der Filamente gegen Unendlich gehen und leitet unter Verwendung asymptotischer Methoden für

jeden Effekt Energiefunktionale her, welche die Filamentpositionen versuchen zu minimieren. Die Idee ist nun, mit Hilfe von Myosin den stationären Zustand zu destabilisieren und in einen beweglichen umzuwandeln. Für Myosin wird angenommen, dass es einerseits aufgrund seiner Steifheit die Filamente in Richtung eines Winkels von 180 Grad drängt und diese andererseits gegeneinander verschiebt. Gleichzeitig kann das Myosinfilament selbst wachsen. Die Kräfte, die es ausübt, wurden daher größenabhängig modelliert. Ein Variationsansatz führt schließlich zu einer Euler-Lagrange Gleichung. Der nächste Schritt wäre, die Myosinterme in einem bestehenden Matlab Code zu implementieren, um zu überprüfen, ob sie zur gewünschten Destabilisierung des stationären Zustandes führen und einen beweglichen Zustand einleiten können.

1 Introduction and Biological Background

1.1 Laboratory Work

Parallel to this diploma thesis I worked on my bachelor's thesis for "Molecular Biology", my second degree which I also study at the University of Vienna. The topics of the two go hand in hand: For the bachelor's thesis I worked with keratocyte cells (see Section 1.6 for more information) in the laboratory of Prof. John Victor Small at the IMBA, Vienna ¹. These cells cannot be kept alive for more than a few days and therefore need to be picked from fresh fish regularly. My work included

- collecting the fish scales and harvesting the keratocytes which live on them
- finding the best method to produce cytoplasts (fragments)
- staining for actin, myosin and the nucleus using fluorescent labeling methods
- producing and examining 2D and 3D electron microscopy pictures to reveal the actin structure

Part of the produced results I used to justify mathematical modeling assumptions (see Chapter 3). My work is part of a bigger project on understanding cellular movement for which there exists a close cooperation between the group of Prof. Christian Schmeiser from the Faculty of Mathematics ² of the University of Vienna and the group of Prof. Victor Small at the IMBA.

In this chapter as well as in Chapter 3 I present some pictures produced mainly during my work at the IMBA. Details about the experiments and their results can be found in my bachelor's thesis.

The rest of this chapter is based on Alberts et al. [2002] with small additions from Berg et al. [2003].

1.2 Mobility and the Cytoskeleton

Many cells, whether unicellular or part of a large ensemble (such as the human) have the ability to actively move from one place to another. A unicellular organism might be able to move towards a source of food or away from danger. During the development of each organism all cells have to be able to move to the right place. Pathogens move from one target cell to the next, immune cells have to be able to crawl to the place of an infection to fight it. Furthermore some cells have to be able to change their shape, for example to divide into two or contract a muscle.

The structural basis of these functions are bundles, networks, etc. formed by long rod-like structures called filaments of various length and diameter which together form the cytoskeleton. Some of its functions partly resemble the functions of our own (bony) skeleton: It gives the cell shape and internal structure, makes them physically robust to outer mechanical stress and is the basis of all movement. However, one big principal difference is that the cytoskeleton is a highly

¹<http://www.imba.oeaw.ac.at>

²<http://plone.mat.univie.ac.at/>

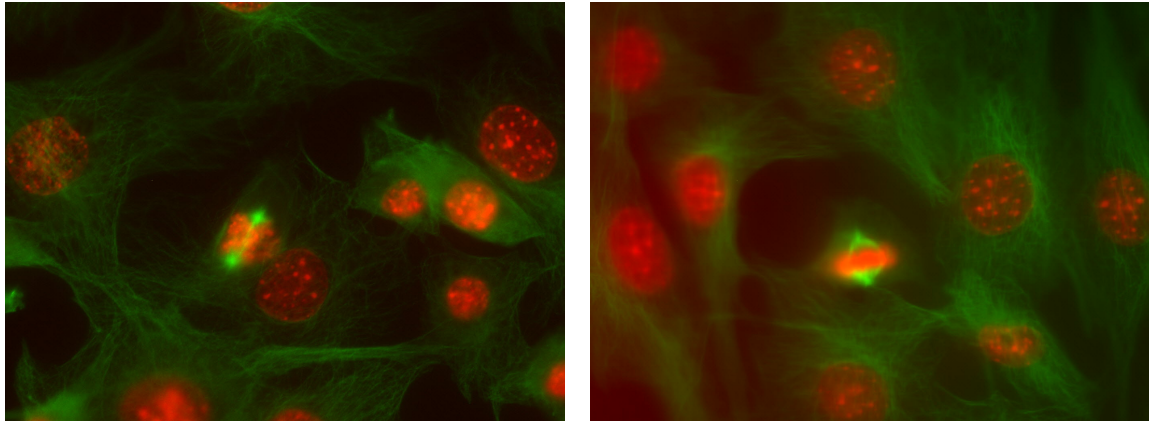


Figure 1.1: The picture shows two stages of mitosis (=cell division) in fibroblasts. DNA is labeled with a red fluorescence marker, microtubuli with a green one. Left picture: the cell in the middle is just at the onset of mitosis (prophase, early metaphase). The two spindle poles form at opposite ends of the nucleus. Right picture: The chromosomes are already lined up between the poles and are about to be separated. Source: self-made, 2010

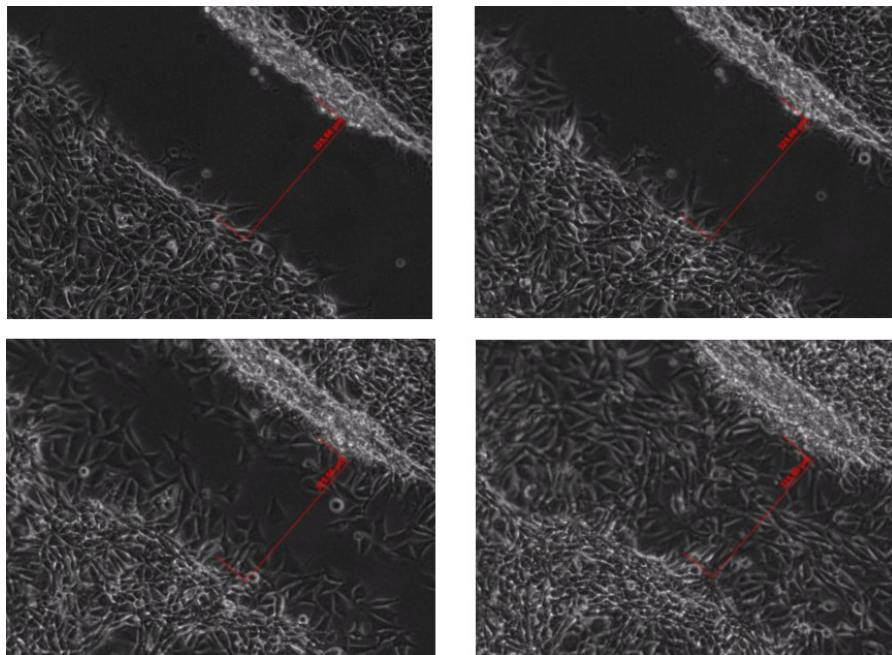


Figure 1.2: The migration of fibroblasts over a gap of $325\mu m$. Source: Self-made, 2010

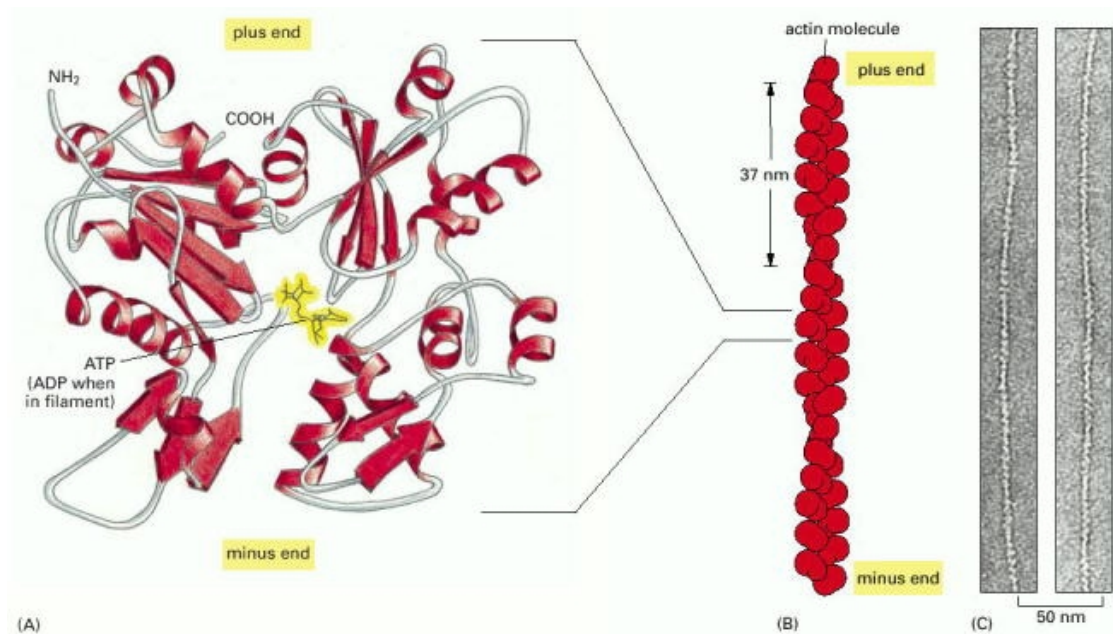


Figure 1.3: An actin filament and its globular subunit. The arrows and helices in the subunit represent amino acid substructures. Source: [Alberts et al. 2002, p. 916]

dynamic structure which can adapt to a large variety of situations. This passage from [Alberts et al. 2002, p. 907] nicely outlines its significance :

The cytoskeleton pulls the chromosomes apart at mitosis (see 1.7) and then splits the dividing cell in two. It drives and guides the intracellular traffic of organelles, plasma membrane and provides the mechanical linkage that let the cell bear stresses and strain without being ripped apart as the environment shifts and changes. It enables some cells, such as sperm to swim, and others, such as fibroblasts and white blood cells, to crawl across surfaces. It provides the machinery in the muscle cells for contraction and in the neuron to extend an axon and dendrites. It guides the growth of the plant cell wall and controls the amazing diversity of eucaryotic shapes.

Here the three types of filaments are mentioned, but we'll be mainly concerned with the first:

- a) Actin Filaments
- b) Intermediate Filaments
- c) Microtubuli

Figure 1.1 and Figure 1.2 show two examples: In the first, one can observe two stages of cell division (mitosis - see 1.7) in fibroblasts (cells of the connective tissue). Here microtubuli play an essential role by forming a so-called spindle that pulls the chromosomes on opposing sides in the cell. The second figure shows how fibroblasts can crawl over a gap. This movement is actin dependent.

1.3 Actin

Actin filaments (F-actin) are protein (see 1.7 for more explanations) homo-polymers consisting of globular actin subunits, which will be referred to as G-actin (see Figure 1.3). The protein G-actin is found in all eukaryotic cells (see 1.7) and is remarkably well preserved across different species. Between two species the amino acid sequences that the protein is made up of are usually about 90% identical. The likely reason for this similarity also reveals part of the importance of actin: Actin has usually many interaction partners ranging from myosins over regulatory proteins to other cytoskeletal proteins. Whenever in the course of evolution the DNA encoding the actin genes were altered (by mutation) in a way that effected the amino acid sequence, this was likely to lead to functional problems with some binding partners. Therefore the likelihood of having damaged a process crucial for the cell's survival was very high. So changing binding partners instead of actin just seems to have been the "safer" way for evolution.

Actin filaments are formed by polymerization which results in two-stranded helical polymers which have a diameter of about 5-9nm. Two main aspects of F-actin are that it is:

- a) polarized
- b) dynamic

The polarization stems from the fact that G-actin is not symmetric, a property which is inherited by F-actin. As a result F-actin has two ends, here referred to as barbed and pointed end. The barbed end grows faster than the pointed end.

As addition is always dependent on the concentration of free monomers, polymerization and depolymerization can happen at both ends. The concentration at which the rate of subunit addition equals the rate of subunit loss is called "Critical Concentration", C_c . A lower concentration would result in a net loss of subunits, a higher one in a net gain. So far, the two ends, despite their different polymerization rates, would still have to have the same C_c , but there is an additional effect involved:

Actin monomers that are added carry a bound ATP (see 1.7 for more explanations). This ATP gets hydrolyzed to ADP shortly after the subunit is incorporated into the filament. Monomers carrying ATP are more difficult to remove from the filament. Therefore, if polymerization is faster than hydrolysis, this results in a protective ATP-cap.

This, together with the differences in rates described above, leads to different critical concentrations at the barbed and pointed end: $C_c(\text{barbed}) < C_c(\text{pointed})$. Therefore if the concentration is between these two, there is a net assembly at the plus end and a net disassembly at the minus end, resulting in so called "treadmilling": The length of the filament stays the same, while each new monomer added at the barbed end gradually moves through the filament to finally detach at the pointed end (see Figure 1.4).

F-actin plays an important role in many cellular processes. It can be arranged in bundles, planar networks and 3-dimensional gels. Here some examples:

- The network gives stability to the cell and helps in signal transduction.
- When a cell divides, a contractile actin-ring forms, which helps splitting the cytoplasm during cytokinesis.
- Spike-like structures on the cell surface like filopodia consist of actin and are used to explore a cell's surrounding.
- By lamellipodia, which are sheetlike structures, a cell can drag itself forward. Inside, the lamellipodium consists of a network of F-actin.

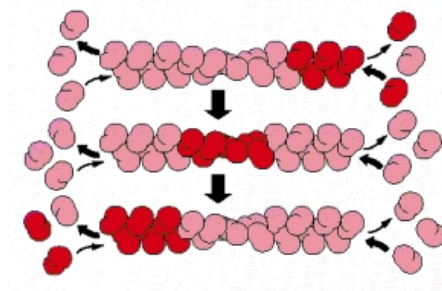


Figure 1.4: A treadmilling actin filament. The sequence shows the path of some monomers through the filament. Source: [Alberts et al. 2002, p. 913]

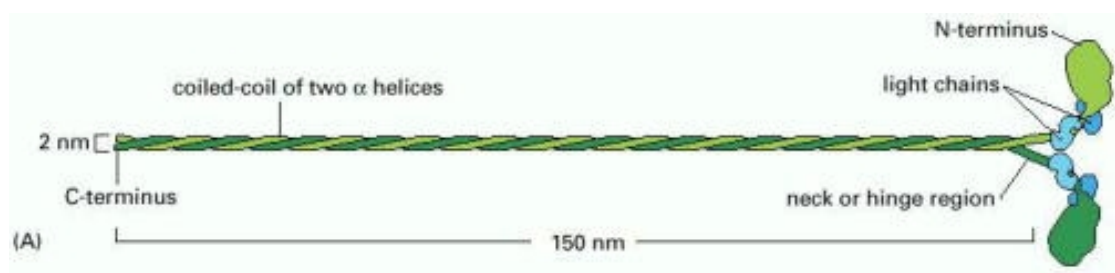


Figure 1.5: The structure of a Myosin II dimer. Source: [Alberts et al. 2002, p. 950]

- Actin bundles of stereocilia can be found on hair in our inner ear and are necessary for hearing.
- Muscular contraction is enabled by an interaction of actin, myosin and other proteins.
- Actin is also involved in the cell movement which allows macrophages to engulf bacterial pathogens.

1.4 Myosin

Of course the cytoskeleton cannot perform its functions without a range of accessory proteins, which can modify and use it.

Myosin is part of a group of proteins associated with the cytoskeleton called "motor proteins". This group has in common that they bind to cytoskeletal fibres such as actin and microtubuli and move along them. The movement results from conformation changes (see 1.7) triggered by ATP hydrolysis and is therefore an energy consuming process. Myosin binds to actin.

There exist several types of myosin, but we will primarily be concerned with myosin II. All the following refers to myosin II, but we will write only myosin for simplicity. Structurally myosin consists of three amino acid chains, one heavy chain and two different light chains. The long helical part of the heavy chain forms the "tail", followed by a "neck" or "hinge" region providing flexibility. On its other end a globular "head" is formed by part of the heavy chain and the two light chains, an essential light chain and a regulatory one. This head serves as the "motor

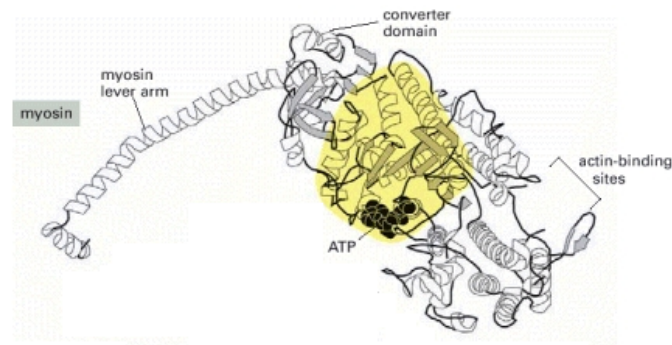


Figure 1.6: The different domains of the head region of myosin. Source: Adapted from [Alberts et al. 2002, p. 953]

domain" which drives the movement. Two such units can form a dimer by wrapping their tails around each other in a structure called "coiled-coil" (see Figures 1.5 and 1.6).

How can myosin move along an actin filament? The movement is made possible by cycling through different states defined by whether ATP or ADP or none of them is bound (see Figure 1.7) :

- a) **Attached:** The head is bound to actin in a rigor conformation (the name stems from "rigor mortis", the stiffness of muscles observed in dead people, which comes precisely from attached myosin heads not letting go)
- b) **Released:** ATP binds to the head, which reduces its affinity for actin
- c) **Cocked:** Without attachment the head moves about 5nm towards the barbed end of actin, then ATP is hydrolyzed, but the products, ADP and P_i remain bound
- d) **Force generating:** Myosin binds weakly to actin, the P_i is released which results in a tight binding. Next ADP is released and while staying bound the head moves back to its original conformation and drags actin along (if possible)
- e) **Attached** again ...

1.5 Interaction in Muscles

In this section the skeletal muscle is used as an (impressive) example of how this interaction between myosin and actin can be used.

The structural unit of a skeletal muscle is a sarcomere (see Figures 1.8 and 1.9). It is highly organized and consists, apart from actin and myosin, of many additional proteins, which allow to tightly regulate and control, when and if a muscle is contracted or relaxed. The sarcomere's two ends are formed by flat structures called Z-discs. On each Z-disc several actin filaments of equal length are attached with their barbed end. Their (free) pointed ends point towards each other and are stabilized by additional proteins in order to avoid (de)polymerization. Between them are thick, symmetric myosin bundles, consisting of many myosins. Some point towards the one Z-disc, some to the other, but all are attached with each other via their tails, such that only the many heads stick out of the bundle on each side.

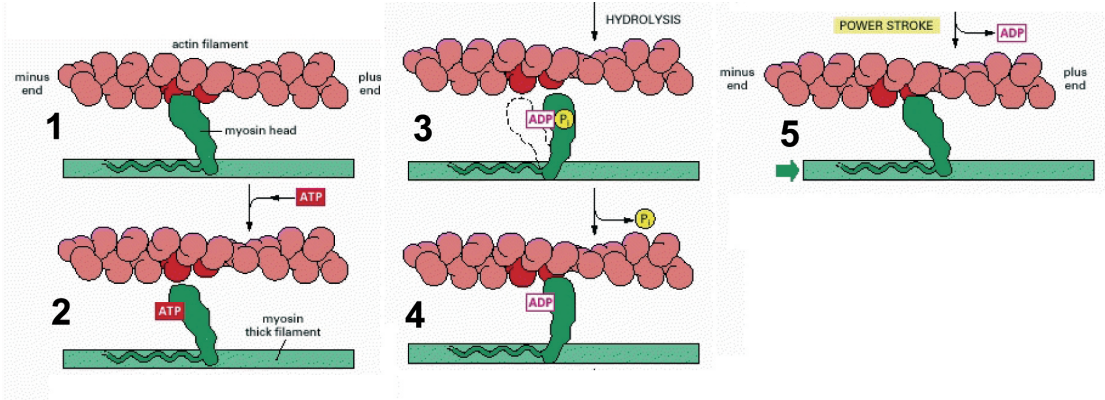


Figure 1.7: Myosin cycles through different conformations while consuming energy. Source: Adapted from [Alberts et al. 2002, p. 955]

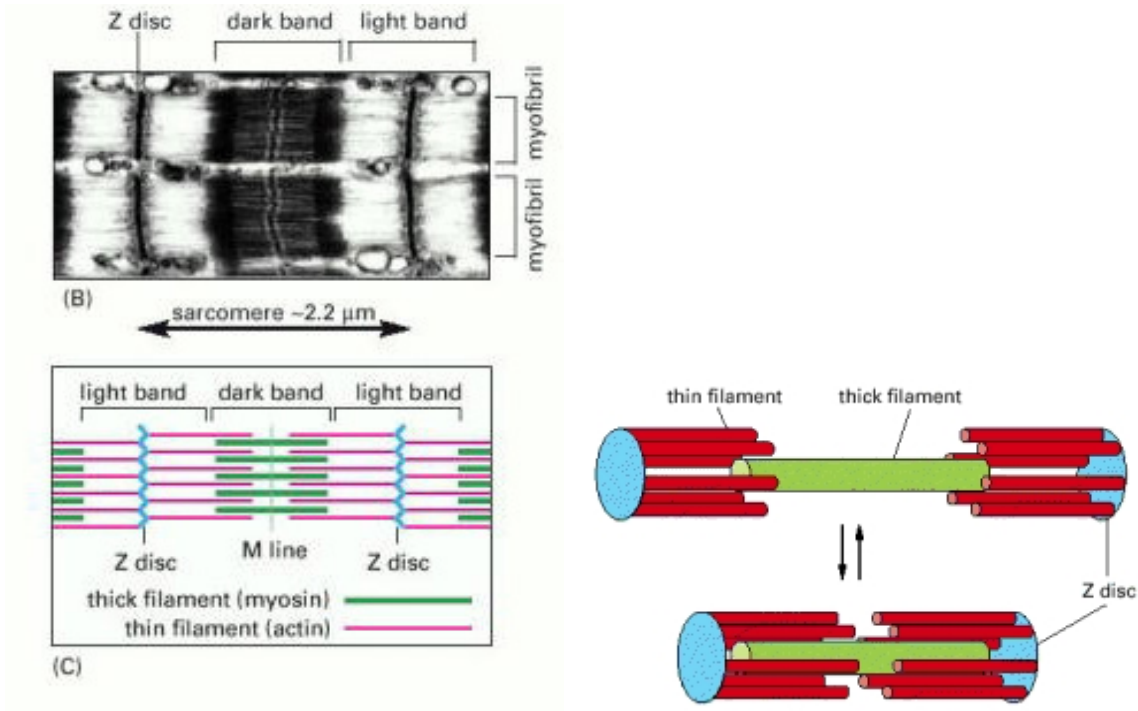


Figure 1.8: The upper left picture shows the electron micrograph of a small part of a skeletal muscle. It contains one whole sarcomere and partly the two bordering sarcomeres. Below a schematic version of the above. On the right the principle of sarcomere contraction is illustrated. Source: Adapted from [Alberts et al. 2002, p. 962-963]

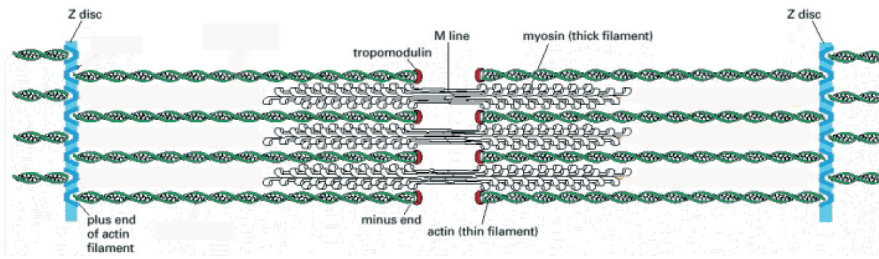


Figure 1.9: A detailed schematic drawing of one sarcomere with (thin) actin filaments and (thick) myosin bundles. Source: Adapted from [Alberts et al. 2002, p. 963]

If the sarcomere receives a signal to contract, each myosin head can start moving along the actin filament by the process described above and tries to move towards the corresponding barbed end. A singular head usually falls off after one step. However, because there are many heads, there are always some that are attached. In effect, because of the heads on the left, the myosin bundle wants to move to the left, but at the same time the heads on the right pull to the right. Because the bundle itself cannot be stretched, this causes the actin filaments together with the attached Z-discs to move towards each other, resulting in a contraction of the sarcomere.

A long chain of these contractile units forms one myofibril, many of which make up a muscle. A myofibril can be as long as the muscle itself and even though the length difference caused by contraction in one sarcomere is small, together they can enable the myofibril and therefore the muscle to change size on a much larger length scale.

1.6 Lamellipodium

In this Chapter 3 we want to model the effect of actin-myosin interaction on the lamellipodial network in keratocyte cytoplasm. Keratocytes are cells that live on the scales of fish, e.g. the samlet. From there they can be collected and cultured for a few days. Keratocytes are very useful model cells for studying cell mobility, because they move fast, without stimulus and in a very characteristic manner. To move they use thin ($0.2 - 0.3\mu m$) sheet-like protrusions called lamellipodia. These contain a dense actin network and several accessory proteins that control and facilitate the movement. The cell body itself is dragged behind. Keratocytes that do not move are usually round with a lamellipodium that is stretched around the whole cell. If pushed or also because of stochastic fluctuations keratocytes can change to a half-moon shape and start moving. In this state the lamellipodium can only be observed at the front edge. At the back thicker actin bundles can be seen. Figure 1.10 shows several moving keratocytes and one stationary cell. The nucleus is colored blue, the actin network green.

There are several proteins and protein complexes associated with the actin network which are involved in the cell's movement. Different actin filaments can be connected by linker proteins such as *filamin*. Additionally does the network form adhesions with the substrate in which the transmembrane protein *integrin* plays an important role.

Interaction of myosin and actin in the lamellipodium is not as organized and structured as in skeletal muscle cells. The actin filaments can generally have many directions.

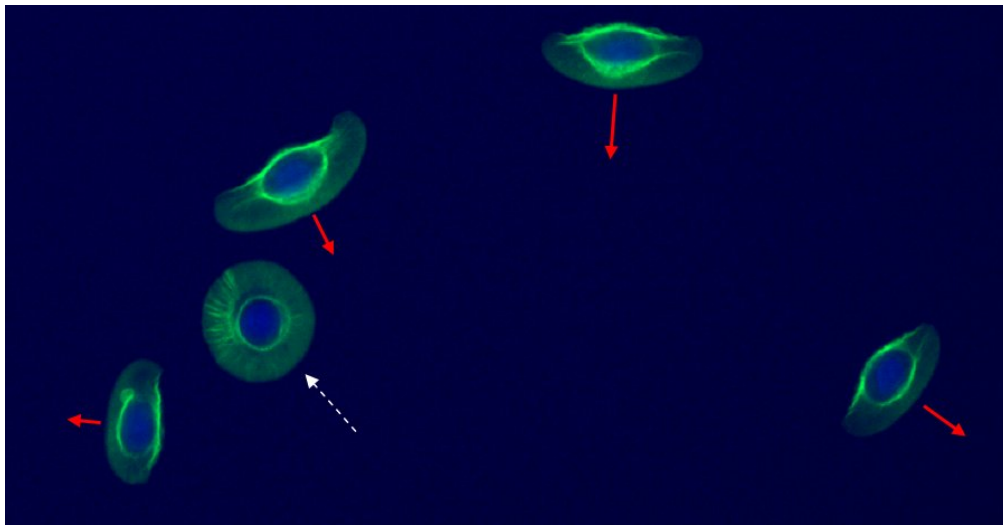


Figure 1.10: Four moving and one stationary keratocyte. Actin is labeled green, the nucleus blue. The red arrow shows the direction of movement, the white arrow points at the round stationary keratocyte. Source: self-made

1.7 Basic Vocabulary

ATP/ADP/Hydrolysis - Adenosine triphosphate (**ATP**) is a universal biochemical "currency". It is a nucleotide and consists of the base adenine attached to the sugar ribose and, most importantly, three phosphate groups. The chemical bonds between the phosphates (phosphoanhydride bonds) are quite stable under various conditions but contain a lot of energy. When a phosphate is removed in a reaction called **hydrolysis** (breakage with involvement of H_2O), this energy is released and can be used to drive other (energy dependent) reactions. The corresponding reaction equation reads: $ATP + H_2O \rightleftharpoons ADP + P_i$. P_i stands for a free phosphate group. The resulting **ADP** (Adenosine diphosphate) contains less energy.

Eukaryotes/Prokaryotes - The coarsest way to classify cells is in prokaryotic and eukaryotic. **Prokaryotic cells**, such as bacteria are very simple in organization and lack specialized structures, such as a nucleus and most cell organelles. A **eukaryote** on the other hand is any other organism (unicellular or multicellular) ranging from yeast to humans.

Protein/Domain/Conformation - A **protein** is a molecule consisting of one or more linear chains of amino acids, that folds into a 3D-shape by several types of forces. The sequence of amino acids that define the protein is encoded in the DNA. The 3D-shape is not rigid, but can be changed when interacting with other substances. Compact globular structural parts of a protein are called **domain** and are defined by their 3D shape. This means that also amino acids that are far apart in the linear chain can become close by protein folding and might therefore be part of the same domain. The different shapes of a protein or a domain are called **conformations**.

Mitosis/Nucleus/Chromosomes - The process of a cell splitting into two is called **mitosis**. It starts after the genetic material organized in **chromosomes** has been duplicated. Then the **nucleus**, which in eukaryotes contains the DNA, dissolves, and a mitotic spindle made from microtubuli forms. The chromosomes align in the middle of the spindle poles and are then pulled apart to be distributed equally to the new daughter cells. The different stages of mitosis are

called Prophase, Metaphase, Anaphase, and Telophase respectively.

2 Modeling of Actin-Myosin Interaction

2.1 Derivation of the Model

In this section we will derive an equation describing the interaction between one end of a myosin bundle with an actin filament (or several aligned actin filaments, which do not move relative to each other). This system is the basis of many mechanisms involving movement, such as muscular action or also the cell movement. All figures in this chapter are self-made.

As described in Chapter 1, myosin bundles move actin via attachment of their heads, followed by a change of conformation, presenting the ATP dependent power stroke.

We consider the actin bundle to be fixed. The position of one attached myosin head on the actin is described by ξ , where $\xi = 0$ represents the point of attachment and $\xi = \xi_0 > 0$ the equilibrium position after the power stroke. v denotes the velocity of the individual myosin head, u the velocity of the whole myosin bundle. As soon as the head attaches, it experiences a number of forces resulting in the following acceleration terms:

- a) a linear spring acceleration $\kappa (\xi_0 - \xi)$, proportional to the head's distance from equilibrium
- b) a friction acceleration $-\eta v$, caused by the environment, e.g. by cytoplasmic drag
- c) a friction acceleration $(u - v)/T$, caused by the fact that one myosin has a resistance to having a different speed than the bundle it is embedded into
- d) an acceleration $-F/m$, caused by an external force holding the bundle back, where the acceleration $F > 0$ is shared by the total number of attached heads.

We call the sum of the above $F_{total}(\xi, v)$. So the movement of one head is determined by $\dot{\xi} = v$, $\dot{v} = F_{total}$.

We look at the distribution function of attached heads $\Psi(\xi, v, t)$ and compute the position dependent number density and flux:

$$\rho(\xi, t) = \int_{-\infty}^{\infty} \Psi(\xi, v, t) dv, \quad j(\xi, t) = \int_{-\infty}^{\infty} v \Psi(\xi, v, t) dv,$$

and furthermore the total number of attached heads $m(t)$, the total stress $\sigma(t)$, and the velocity of the myosin bundle $u(t)$, defined as an average velocity:

$$\begin{aligned} m(t) &= \int_{-\infty}^{\infty} \int_{-\infty}^{\infty} \Psi(\xi, v, t) dv d\xi = \int_{-\infty}^{\infty} \rho(\xi, t) d\xi \\ \sigma(t) &= \kappa \int_{-\infty}^{\infty} \int_{-\infty}^{\infty} (\xi_0 - \xi) \Psi(\xi, v, t) dv d\xi = \kappa \int_{-\infty}^{\infty} (\xi_0 - \xi) \rho(\xi, t) d\xi \\ u(t) &= \frac{1}{m(t)} \int_{-\infty}^{\infty} \int_{-\infty}^{\infty} v \Psi(\xi, v, t) dv d\xi = \frac{1}{m(t)} \int_{-\infty}^{\infty} j(\xi, t) d\xi \end{aligned} \tag{2.1}$$

We want to derive an equation for the distribution function $\Psi(\xi, v, t)$, where

$$\int_B \Psi(\xi, v, t) d\xi dv$$

describes the number of attached heads in B at time t , B being a set in the phase space (ξ, v) . Calculating the change of this quantity and taking into account that only the normal component of the trajectories adds mass, we get:

$$\begin{aligned} \frac{d}{dt} \int_B \Psi(\xi, v, t) d\xi dv &= - \int_{\partial B} \Psi \begin{pmatrix} v \\ F_{total} \end{pmatrix} \cdot n d\sigma + \int_B H d\xi dv \\ &= - \int_B \partial_\xi (\Psi v) + \partial_v (\Psi F_{total}) d\xi dv + \int_B H d\xi dv \end{aligned} \quad (2.2)$$

where H is the difference between the attachment and detachment densities, i.e. describes source and sink terms. For the second equality the divergence theorem has been used. As this remains true for arbitrary sets B , we conclude equality of the integrands.

Concerning the dynamics of detached heads, we make the simplifying assumption that they immediately after detachment assume the cocked state and move with the bundle velocity u . This implies that attachment always happens at $\xi = 0$, $v = u$, and that the equilibrium position ξ_0 is constant (and equal to the equilibrium length of the power stroke).

The attachment and detachment rate are assumed to have the form $f(u)$ and, respectively, $g(u)$. Using this and (2.2) we finally get the following non-linear transport equation:

$$\begin{aligned} \partial_t \Psi + v \partial_\xi \Psi + \partial_v \left[\left(\kappa (\xi_0 - \xi) - \eta v + \frac{u(t) - v}{T} - \frac{F}{m(t)} \right) \Psi \right] \\ = \delta(\xi) \delta(v - u(t)) f(u(t)) (N - m(t)) - g(u(t)) \Psi \end{aligned} \quad (2.3)$$

where N is the total number of (attached and detached) myosin heads.

It is remarkable that from this equation a closed system for the moments $m(t)$, $u(t)$ and $\sigma(t)$ can be derived. To see that, we first integrate (2.3) with respect to v . Using integration by parts together with the (natural) assumption that Ψ and all its moments vanish far out we get:

$$\partial_t \rho + \partial_\xi j = \delta(\xi) f(u) (N - m) - g(u) \rho \quad (2.4)$$

A further integration of (2.4) with respect to ξ gives:

$$\dot{m} = f(u) (N - m) - g(u) m \quad (2.5)$$

Now we multiply (2.3) by v and integrate with respect to v and ξ . We use the fact that $-\iint \frac{u-v}{T} \Psi dv d\xi = -\frac{u}{T} m + \frac{1}{T} u m = 0$ and find:

$$(\dot{m} u) - \sigma + \eta m u + F = u f(u) (N - m) - g(u) m u$$

Combining this with (2.5) we get:

$$\dot{u} = \frac{\sigma}{m} - \eta u - \frac{F}{m} \quad (2.6)$$

Finally we multiply (2.4) by $\kappa (\xi_0 - \xi)$ and integrate with respect to ξ :

$$\dot{\sigma} = -\kappa m u + \kappa \xi_0 f(u) (N - m) - g(u) \sigma \quad (2.7)$$

2.2 Analysis of ODE Moment System

From now on we will assume constant attachment and detachment rates. The system (2.5), (2.6), (2.7) has the following form:

$$\begin{aligned} \dot{m} &= f(N - m) - gm, \\ \dot{u} &= \frac{\sigma}{m} - \eta u - \frac{F}{m}, \\ \dot{\sigma} &= -\kappa m u + \kappa \xi_0 f(N - m) - g\sigma. \end{aligned} \tag{2.8}$$

Now we are in a special situation, because we can work with the moment system without any knowledge about the distribution function Ψ . From (2.8) we get the following steady states:

$$\begin{aligned} \bar{m} &= \frac{Nf}{g+f} \\ \bar{u} &= \frac{g}{\kappa + g\eta} \left(\kappa \xi_0 - \frac{F(f+g)}{Nf} \right) \\ \bar{\sigma} &= \eta \bar{m} \bar{u} + F \end{aligned} \tag{2.9}$$

Linearizing the system at these steady states gives:

$$\begin{pmatrix} \dot{m} \\ \dot{u} \\ \dot{\sigma} \end{pmatrix} = \begin{pmatrix} -f-g & 0 & 0 \\ -\frac{\bar{\sigma}}{\bar{m}^2} + \frac{F}{\bar{m}^2} & -\eta & \frac{1}{\bar{m}} \\ -\kappa \bar{u} - \kappa \xi_0 f & -\kappa \bar{m} & -g \end{pmatrix} \begin{pmatrix} m - \bar{m} \\ u - \bar{u} \\ \sigma - \bar{\sigma} \end{pmatrix}$$

We get as eigenvalues for the matrix:

$$\begin{aligned} \mu_1 &= -(f+g) \\ \mu_2 &= -\frac{1}{2}(g+\eta) + \sqrt{\frac{1}{4}(g+\eta)^2 - (\kappa + \eta g)} \\ \mu_3 &= -\frac{1}{2}(g+\eta) - \sqrt{\frac{1}{4}(g+\eta)^2 - (\kappa + \eta g)} \end{aligned}$$

The real parts of all three eigenvalues are negative, therefore the steady states are locally stable. This means that the moments $m(t)$, $u(t)$ and $\sigma(t)$ will converge to \bar{m} , \bar{u} and $\bar{\sigma}$, if their initial conditions lie in a neighborhood of $(\bar{m}, \bar{u}, \bar{\sigma})$.

However, we can do better than that and aim for global stability: First of all we note that the equation for $m(t)$ in (2.8) is not coupled with the rest and can be solved explicitly to give $m(t) = \bar{m} + e^{-(f+g)t}(m_0 - \bar{m})$. Convergence to \bar{m} for all initial conditions m_0 is clear, however one should choose $0 < m_0 \leq N$. $m = 0$ is excluded because it causes problems in the equation for $u(t)$. For $u(t)$ and $\sigma(t)$ some more work is required. An important observation is, that the nonlinearity in (2.8) stems from $m(t)$. Therefore we can rewrite the ODEs for u and σ as a linear, but no longer autonomous system. For the following we introduce the abbreviations $x(t) := (u(t), \sigma(t))$ and $\bar{x} := (\bar{u}, \bar{\sigma})$:

$$\begin{aligned} \dot{x}(t) &= B(t)x(t) + b(t) \\ B(t) &:= \begin{pmatrix} -\eta & \frac{1}{m(t)} \\ -\kappa m(t) & -g \end{pmatrix} \\ b(t) &:= \begin{pmatrix} -\frac{F}{m(t)} \\ \kappa \xi_0 f(N - m(t)) \end{pmatrix} \end{aligned} \tag{2.10}$$

We know that for large times the dependence of B and b on t will decrease. The key idea now is to interpret (2.10) as a perturbed system, with an autonomous unperturbed part and a time dependent perturbation. This idea results in a splitting of $B(t)$ and $b(t)$ in their limits \bar{B} and \bar{b} and remainders $R(t)$ and $r(t)$ which tend to zero as $t \rightarrow \infty$. In formulas this looks as follows:

$$\begin{aligned} B(t) &= \bar{B} + R(t) = \begin{pmatrix} -\eta & \frac{1}{\bar{m}} \\ -\kappa\bar{m} & -g \end{pmatrix} + \begin{pmatrix} 0 & \frac{\bar{m}-m(t)}{\bar{m}m(t)} \\ \kappa(\bar{m}-m(t)) & 0 \end{pmatrix} \\ b(t) &= \bar{b} + r(t) = \begin{pmatrix} -\frac{F}{\bar{m}} \\ \kappa\xi_0 f(N-\bar{m}) \end{pmatrix} + \begin{pmatrix} -\frac{F}{m(t)\bar{m}}(\bar{m}-m(t)) \\ \kappa\xi_0 f(\bar{m}-m(t)) \end{pmatrix} \end{aligned}$$

Defining $h := f + g > 0$ it is easy to check that:

$$\begin{aligned} \|R(t)\| &\leq R_0 e^{-ht} \\ |r(t)| &\leq r_0 e^{-ht} \end{aligned} \tag{2.11}$$

with positive constants R_0 and r_0 . $\|\cdot\|$ defines the operator norm induced by the Euclidean vector norm $|\cdot|$.

The eigenvalues of \bar{B} are μ_2 and μ_3 from above, which have negative real parts. Therefore we can estimate:

$$\|e^{\bar{B}t}\| \leq C e^{-\rho t} \tag{2.12}$$

with positive constants C and ρ .

In a first step we show that $|x(t)|$ is bounded. To this end we need the following version of the Gronwall's inequality (see Teschl), which states that for a real valued function $y(t)$ satisfying

$$\begin{aligned} y(t) &\leq \alpha(t) + \int_0^t \beta(s)y(s)ds \\ s \leq t &\implies \alpha(s) \leq \alpha(t) \end{aligned} \tag{2.13}$$

with real valued functions $\alpha(s)$ and $\beta(s)$ we can conclude that

$$y(t) \leq \alpha(t) \exp\left(\int_0^t \beta(s)ds\right). \tag{2.14}$$

Writing $\dot{x}(t) = \bar{B}x(t) + \bar{b} + R(t)x(t) + r(t)$ and interpreting $\bar{b} + R(t)x(t) + r(t)$ as inhomogeneity the variation of constants approach gives

$$x(t) = e^{\bar{B}t}x_0 + \int_0^t e^{\bar{B}(t-s)}\bar{b}ds + \int_0^t e^{\bar{B}(t-s)}R(s)x(s)ds + \int_0^t e^{\bar{B}(t-s)}r(s)ds. \tag{2.15}$$

Next we use the estimates (2.11) and (2.12) and define $y(t) := |x(t)|e^{\rho t}$.

$$\begin{aligned} |x(t)| &\leq C e^{-\rho t}|x_0| + C|\bar{b}| \int_0^t e^{-\rho(t-s)}ds + C R_0 \int_0^t e^{-\rho(t-s)}|x(s)|e^{-hs}ds + C r_0 \int_0^t e^{-\rho(t-s)}e^{-hs}ds \\ y(t) &\leq C|x_0| + C|\bar{b}| \int_0^t e^{\rho s}ds + C R_0 \int_0^t e^{-hs}y(s)ds + C r_0 \int_0^t e^{(\rho-h)s}ds \end{aligned}$$

To apply Gronwall's inequality we define:

$$\alpha(t) := C|x_0| + C|\bar{b}| \int_0^t e^{\rho s}ds + C r_0 \int_0^t e^{(\rho-h)s}ds$$

$$\begin{aligned}
 &= C|x_0| + \frac{C|\bar{b}|}{\rho} (e^{\rho t} - 1) + \frac{C r_0}{\rho - h} (e^{(\rho-h)t} - 1) \\
 &= C_1 + C_2 e^{\rho t} + C_3 e^{(\rho-h)t} \\
 \beta(s) &:= C R_0 e^{-h s} \\
 \int_0^t \beta(s) ds &= \frac{C R_0}{h} (1 - e^{-h t}) = C_4 (1 - e^{-h t})
 \end{aligned}$$

We see that $y(t)$ fullfills the two conditions in (2.13). $\alpha(t)$ grows in t because it is defined as integrals of non-negative functions from 0 to t . Note that having $\rho - h$ in the denominator doesn't cause problems, because ρ in (2.12) can be chosen differently as long as it is smaller than $\min\{-Re(\mu_2), -Re(\mu_3)\}$. C would then change too.

Now we apply (2.14) and find that:

$$\begin{aligned}
 y(t) &\leq \left(C_1 + C_2 e^{\rho t} + C_3 e^{(\rho-h)t} \right) \exp(C_4 (1 - e^{-h t})) \\
 |x(t)| &\leq (C_1 e^{-\rho t} + C_2 + C_3 e^{-h t}) \exp(C_4 (1 - e^{-h t})) \leq M
 \end{aligned}$$

for some $M > 0$. This shows that $|x(t)|$ is bounded. To show $\lim_{t \rightarrow \infty} x(t) = \bar{x}$ we notice that the unperturbed system converges to \bar{x} , that is:

$$\begin{aligned}
 \dot{z}(t) &= \bar{B}z(t) + \bar{b} \\
 z(t) &= e^{\bar{B}t} x_0 + \int_0^t e^{\bar{B}(t-s)} \bar{b} ds \\
 |z(t) - \bar{x}| &\rightarrow 0 \text{ for } t \rightarrow \infty
 \end{aligned}$$

Now we use this information in (2.15) and together with $|x(t)| \leq M$ we find that:

$$\begin{aligned}
 |x(t) - \bar{x}| &\leq |z(t) - \bar{x}| + (C R_0 M + C r_0) e^{-\rho t} \int_0^t e^{(\rho-h)s} ds \\
 &\leq |z(t) - \bar{x}| + C_5 (e^{-h t} - e^{-\rho t}) \rightarrow 0 \text{ for } t \rightarrow \infty
 \end{aligned}$$

This finishes the proof of the global stability of the steady states \bar{u} and $\bar{\sigma}$. In the following all we need to assume about the initial head distribution $\Psi_0(\xi, v)$ is that its moments m_0 , u_0 and σ_0 exist with $0 < m_0 \leq N$.

Figure 2.1 shows the graphs of $m(t)$, $u(t)$ and $\sigma(t)$ for certain parameters with small initial conditions for all three.

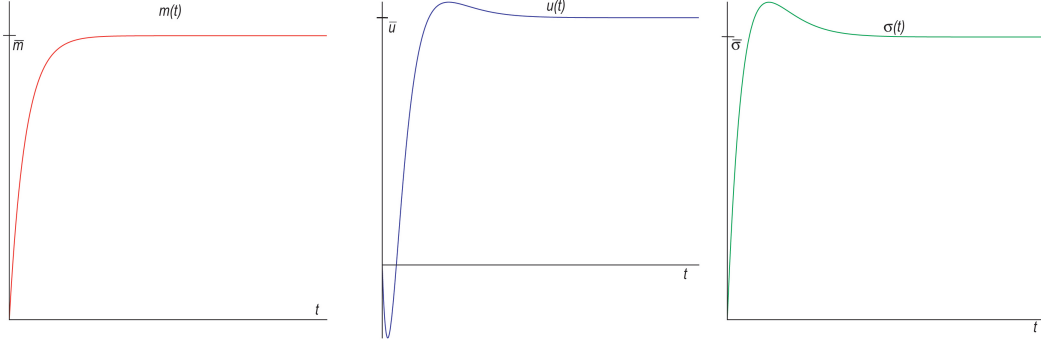
2.3 Stationary Equation

Again we will assume the attachment and detachment rates f and g to be independent of u . The stationary equation now takes the form:

$$v \partial_\xi \bar{\Psi} + \left[-\kappa \xi - \left(\eta + \frac{1}{T} \right) v + \overline{Inh} \right] \partial_v \bar{\Psi} = r \bar{\Psi} + \delta(\xi) \delta(v - \bar{u}) \hat{f} \quad (2.16)$$

with

$$r := -g + \eta + \frac{1}{T} \quad (2.17)$$


 Figure 2.1: The moments $m(t)$, $u(t)$ and $\sigma(t)$ for certain parameters

$$\begin{aligned}\overline{Inh} &:= \kappa\xi_0 + \frac{\bar{u}}{T} - \frac{F}{\bar{m}} \\ \hat{f} &:= f(N - \bar{m})\end{aligned}$$

The variables \bar{u} and \bar{m} are now known, independent of t and take their values from the stationary solutions in (2.9).

What kind of solutions will we get? As there are Delta distributions in the equation we cannot hope for strong, smooth solutions, but will generally work with weak formulations. To show existence and uniqueness we will approximate δ by a bounded approximation δ_ϵ .

We will solve for each ϵ and then take the limit $\epsilon \rightarrow 0$. For easier calculations we will use the following regularization:

$$\delta_\epsilon(z) = \begin{cases} \frac{1}{2\epsilon} & |z| \leq \epsilon \\ 0 & \text{else} \end{cases} \quad (2.18)$$

This poses the questions whether the corresponding u_ϵ and m_ϵ (and their corresponding stationary solutions) look differently. When one looks at the derivation of the ODE system for u , σ and m one sees that the only properties of δ that enter the calculations are the facts that its integral is 1 and that its first moment is 0. Both characteristics are fulfilled by the approximation, therefore \bar{u} and \bar{m} do not change their values in the regularized equation.

We solve by using the method of characteristics. Changing from (ξ, v) to (s, w) where s is the parameter along the characteristics and w describes, where the characteristics start, we get:

$$\begin{pmatrix} \dot{\xi} \\ \dot{v} \end{pmatrix} = A \begin{pmatrix} \xi \\ v \end{pmatrix} + \begin{pmatrix} 0 \\ \overline{Inh} \end{pmatrix}$$

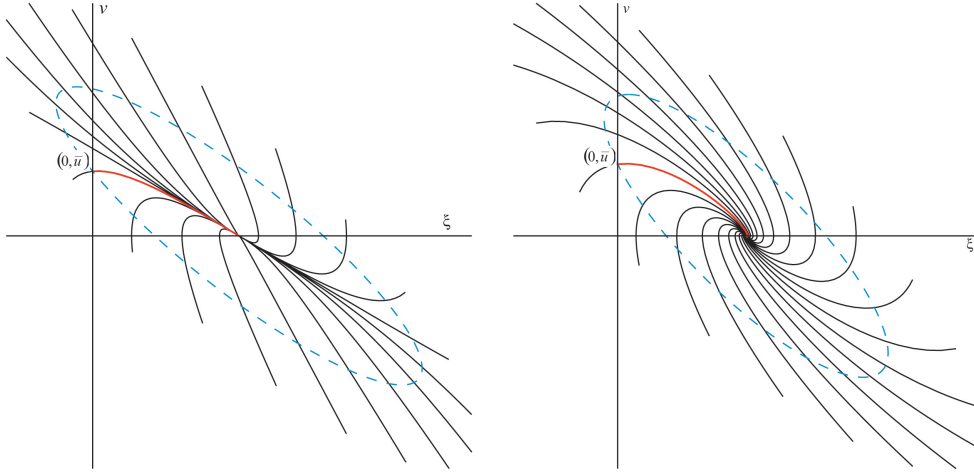
With $A := \begin{pmatrix} 0 & 1 \\ -\kappa & -\eta - \frac{1}{T} \end{pmatrix}$. The dot describes derivation with respect to s . The eigenvalues of

A are $\lambda_{1,2} = -\frac{1}{2}(\eta + \frac{1}{T}) \pm \sqrt{\frac{1}{4}(\eta + \frac{1}{T})^2 - \kappa}$.

2.3.1 The Characteristics

The characteristics take the form:

$$\begin{pmatrix} \xi(w, s) \\ v(w, s) \end{pmatrix} = e^{As} \begin{pmatrix} \xi_0(w) \\ v_0(w) \end{pmatrix} + e^{As} \bar{C}(s) \quad (2.19)$$


 Figure 2.2: The characteristics in the (ξ, v) -plane for real and complex eigenvalues

$$\bar{C}(s) := \int_0^s e^{-Ar} \begin{pmatrix} 0 \\ \frac{0}{Inh} \end{pmatrix} dr$$

The real parts of the eigenvalues of A , λ_1 and λ_2 , are always negative. Therefore taking $s \rightarrow \infty$ we get convergence of all characteristics to:

$$\begin{pmatrix} \xi \\ v \end{pmatrix} = -A^{-1} \begin{pmatrix} 0 \\ \frac{0}{Inh} \end{pmatrix} = \begin{pmatrix} \frac{Inh}{\kappa} \\ 0 \end{pmatrix}$$

Figure 2.2 shows the characteristics in the (ξ, v) -plane for real and complex eigenvalues. The importance of red characteristic will be explained below. The ellipse in the picture shows where the characteristics start. If the solution is prescribed there, one has to make sure that the sub-manifold $w \mapsto \xi_0(w), v_0(w)$ is never tangential to the characteristics. One way to ensure that and at the same time simplify the characteristics' equations, is to take into account the geometry of the system. The idea is to transform the system into its canonical shape using the change of basis matrix the brings A in Jordan normal form. In the new system initial conditions are defined on a circle, which corresponds to an ellipse in the original system. For details see 2.6.1

With this idea a suitable sub-manifold for the initial conditions can be found and defined in a way such that:

$$(\xi(0, 0), v(0, 0)) = (0, \bar{u}) \tag{2.20}$$

The Jacobian $\begin{pmatrix} \partial_w \xi & \partial_s \xi \\ \partial_w v & \partial_s v \end{pmatrix}$ has a determinant, which we call $J(w, s)$, with the following shape:

$$J(w, s) = R(w)e^{s(\lambda_1 + \lambda_2)} \neq 0 \tag{2.21}$$

for some function $R(w)$ depending on the type of eigenvalues (real, complex, two-fold). Note that because the map $(w, s) \mapsto (\xi, v)$ is bijective, also the inverse statement to (2.20) is true, i.e. $(w(0, \bar{u}), s(0, \bar{u})) = (0, 0)$. We define $J_0 := J(w = 0, s = 0)$

2.3.2 Calculating the Stationary Solution

We return to the equation for $\bar{\Psi}$, written in terms of characteristic coordinates:

$$\dot{\bar{\Psi}}_\epsilon = r\bar{\Psi}_\epsilon + \hat{f}\delta_\epsilon(\xi)\delta_\epsilon(v - \bar{u})$$

To obtain the particular solution using the variation of constants approach ($\bar{\Psi}_\epsilon^{part}(w, s) = c_\epsilon(w, s)e^{rs}$), one needs to calculate

$$c_\epsilon(w, s) = \hat{f} \int_{-\infty}^s e^{-rt} \delta_\epsilon(\xi(w, t)) \delta_\epsilon(v(w, t) - \bar{u}) dt.$$

As we expect a weak solution we write a weak formulation of the integral with $\phi(w, s)$ a suitable test function (what suitable means here will be specified at the end of the chapter):

$$\begin{aligned} \langle c_\epsilon(w, s), \phi(w, s) \rangle &= \hat{f} \int_0^{2\pi} \int_{-\infty}^{\infty} \int_{-\infty}^s e^{-rt} \delta_\epsilon(\xi(w, t)) \delta_\epsilon(v(w, t) - \bar{u}) dt \phi(w, s) ds dw \\ &= \hat{f} \int_0^{2\pi} \int_{-\infty}^{\infty} e^{-rt} \delta_\epsilon(\xi(w, t)) \delta_\epsilon(v(w, t) - \bar{u}) \int_t^{\infty} \phi(w, s) ds dt dw \\ &= \hat{f} \int_{-\infty}^{\infty} \int_{-\infty}^{\infty} \frac{1}{J(\xi, v)} e^{-rt(\xi, v)} \delta_\epsilon(\xi) \delta_\epsilon(v - \bar{u}) \int_{t(\xi, v)}^{\infty} \phi(w(\xi, v), s) ds d\xi dv \\ &= \frac{\hat{f}}{4\epsilon^2} \int_{\bar{u}-\epsilon}^{\bar{u}+\epsilon} \int_{-\epsilon}^{\epsilon} \frac{1}{J(\xi, v)} e^{-rt(\xi, v)} \int_{t(\xi, v)}^{\infty} \phi(w(\xi, v), s) ds d\xi dv \\ &= \frac{\hat{f}}{4} \int_{-1}^1 \int_{-1}^1 \frac{1}{J(\epsilon y, \epsilon x + \bar{u})} e^{-rt(\epsilon y, \epsilon x + \bar{u})} \int_{t(\epsilon y, \epsilon x + \bar{u})}^{\infty} \phi(w(\epsilon y, \epsilon x + \bar{u}), s) ds dy dx \end{aligned}$$

The second equality is obtained by exchanging the t and the s integrals while still integrating over the same area. The third via a change of variables: $\xi = \xi(w, t)$, $v = v(w, t)$ (as defined in (2.19)), the fourth uses the regularization of the δ s given in (2.18) and finally the fifth via a second change of variables: $x = \frac{v - \bar{u}}{\epsilon}$, $y = \frac{\xi}{\epsilon}$.

Now letting $\epsilon \rightarrow 0$, we use (2.20) and obtain:

$$\begin{aligned} \langle c(w, s), \phi(w, s) \rangle &= \frac{\hat{f}}{J_0} \int_0^{\infty} \phi(0, s) ds \\ &= \frac{\hat{f}}{J_0} \langle H(s)\delta(w), \phi(w, s) \rangle \end{aligned}$$

Putting things together we get:

$$\bar{\Psi}(w, s) = \frac{f(N - \bar{m})}{J_0} \delta(w) H(s) e^{rs} + K(w) e^{rs} \quad (2.22)$$

We see that the solution is concentrated on one part of the characteristic starting in $w = 0$, to be precise, the part that is described by $s \geq 0$. In Figure 2.2 this corresponds to the red line.

The bijective map $(w, s) \rightarrow (\xi(w, s), v(w, s))$ cannot be inverted explicitly.

We expect $K(w) \equiv 0$. To show that we can recalculate the moments of the stationary solution expecting to get back the equilibria in (2.9).

All moments are calculated using the change of variables $w = w(\xi, v)$ $s = s(\xi, v)$. Here just the calculations for total number of attached heads and the average velocity will be carried out. Calculating the total stress is done similarly. We will only use the first part of (2.22), as this already gives the correct moments. From that we can conclude that all moment integrals involving $K(w)$ have to be zero and thereby $K(w) \equiv 0$.

$$\begin{aligned}
 & \int_{-\infty}^{\infty} \int_{-\infty}^{\infty} \bar{\Psi}(w(\xi, v), s(\xi, v)) d\xi dv \\
 &= \int_0^{2\pi} \int_{-\infty}^{\infty} J(w, s) \frac{f(N - \bar{m})}{J_0} \delta(w) H(s) e^{rs} ds dw \\
 &= \frac{f(N - \bar{m}) J_0}{J_0} \int_0^{\infty} e^{-gs} ds \\
 &= \frac{Nf}{f + g} = \bar{m}
 \end{aligned}$$

We use $\lambda_1 + \lambda_2 + r = -g$, (2.9) and (2.21).

Next we calculate the average velocity in a similar way:

$$\begin{aligned}
 & \int_{-\infty}^{\infty} \int_{-\infty}^{\infty} v \bar{\Psi}(w(\xi, v), s(\xi, v)) d\xi dv \\
 &= \frac{f(N - \bar{m})}{J_0} \int_0^{2\pi} \int_{-\infty}^{\infty} v(w, s) \delta(w) H(s) J(w, s) e^{rs} ds \\
 &= f(N - \bar{m}) \int_0^{\infty} v(0, s) e^{-gs} ds
 \end{aligned}$$

At this point we need the equations of the characteristics given in (2.19). For easier calculations we include $\xi(0, s)$ and write a vector equation:

$$\begin{aligned}
 f(N - \bar{m}) \int_0^{\infty} \begin{pmatrix} \xi(0, s) \\ v(0, s) \end{pmatrix} e^{-gs} ds &= f(N - \bar{m}) \left[\underbrace{\int_0^{\infty} e^{As} \begin{pmatrix} 0 \\ \bar{u} \end{pmatrix} e^{-gs} ds}_{K_1} + \underbrace{\int_0^{\infty} e^{As} \bar{C}(s) e^{-gs} ds}_{K_2} \right] \\
 &= \frac{f(N - m)}{g} \left(Id - \frac{1}{g} A \right)^{-1} \begin{pmatrix} 0 \\ \bar{u} + \frac{Inh}{g} \end{pmatrix} \\
 &= \bar{m} \begin{pmatrix} \bar{u} \\ \bar{u} \end{pmatrix}
 \end{aligned}$$

Now we see that the second entry in the last line gives back $\bar{m}\bar{u}$ as claimed. The second equality can be shown by integration by parts of K_1 and K_2 which gives:

$$\begin{aligned}
 K_1 &= \frac{1}{g} \left(Id - \frac{1}{g} A \right)^{-1} \begin{pmatrix} 0 \\ \bar{u} \end{pmatrix} \\
 K_2 &= \frac{1}{g^2} \left(Id - \frac{1}{g} A \right)^{-1} \begin{pmatrix} 0 \\ Inh \end{pmatrix}
 \end{aligned}$$

Id is the matrix identity.

The calculations for the total stress are not shown here but also give back $\bar{\sigma}$.

2.4 Full Equation

Next we will look at the full equation where $u(t)$ and $m(t)$ are now functions defined as in (2.1) and described by the ODE system (2.8). Using the same abbreviations as for the stationary case (2.17), we get:

$$\partial_t \Psi + v \partial_\xi \Psi + \left[-\kappa \xi - \left(\eta + \frac{1}{T} \right) v + Inh(t) \right] \partial_v \Psi = r \Psi + \delta(\xi) \delta(v - u(t)) f(N - m(t)) \quad (2.23)$$

With $\Psi_0(\xi, v) := \Psi(\xi, v, 0)$.

2.4.1 Calculating the Full Solution

To find the solution we again use the methods of characteristics and get

$$\begin{aligned} \begin{pmatrix} \xi(x, y, t) \\ v(x, y, t) \end{pmatrix} &= e^{At} \begin{pmatrix} x \\ y \end{pmatrix} + e^{At} C(t), \\ C(t) &= \int_0^t \left(e^{-Ar} \begin{pmatrix} 0 \\ Inh(r) \end{pmatrix} \right) dr. \end{aligned} \quad (2.24)$$

t is now the time variable. The second part takes the form:

$$\begin{aligned} \xi_{part}(t) &:= \frac{1}{\lambda_1 - \lambda_2} \left(e^{\lambda_1 t} \int_0^t Inh(\tilde{t}) e^{-\lambda_1 \tilde{t}} d\tilde{t} - e^{\lambda_2 t} \int_0^t Inh(\tilde{t}) e^{-\lambda_2 \tilde{t}} d\tilde{t} \right) \\ v_{part}(t) &:= \frac{1}{\lambda_1 - \lambda_2} \left(\lambda_1 e^{\lambda_1 t} \int_0^t Inh(\tilde{t}) e^{-\lambda_1 \tilde{t}} d\tilde{t} - \lambda_2 e^{\lambda_2 t} \int_0^t Inh(\tilde{t}) e^{-\lambda_2 \tilde{t}} d\tilde{t} \right) \end{aligned}$$

For $t \rightarrow \infty$ the characteristics again converge to $\left(\frac{Inh}{\kappa}, 0 \right)$, just as the characteristics in the stationary case.

Unlike the stationary case we can invert the map $(\xi, v, t) \rightarrow (\xi(x, y, t), v(x, y, t))$ explicitly via:

$$\begin{pmatrix} x(\xi, v, t) \\ y(\xi, v, t) \end{pmatrix} = e^{-At} \begin{pmatrix} \xi \\ v \end{pmatrix} - C(t) \quad (2.25)$$

The determinant of the Jacobian becomes:

$$\begin{vmatrix} \partial_t t & \partial_x t & \partial_y t \\ \partial_t \xi & \partial_x \xi & \partial_y \xi \\ \partial_t v & \partial_x v & \partial_y v \end{vmatrix} = |e^{At}| = e^{t(\lambda_1 + \lambda_2)}$$

To calculate the varied constant (see above) we again use a weak formulation:

$$\begin{aligned} &\int_{-\infty}^{\infty} \int_{-\infty}^{\infty} c_\epsilon(x, y, t) \phi(x, y) dx dy \\ &= \int_{-\infty}^{\infty} \int_{-\infty}^{\infty} \int_0^t (N - m(s)) e^{-rs} \delta_\epsilon(\xi(x, y, s)) \delta_\epsilon(v(x, y, s) - u(s)) ds \phi(x, y) dx dy \\ &= \int_0^t \iint (N - m(s)) e^{-(\lambda_1 + \lambda_2 + r)s} \delta_\epsilon(\xi) \delta_\epsilon(v - u(s)) \phi(x(\xi, v, s), y(\xi, v, s)) d\xi dv ds \end{aligned}$$

For the last equality we used a change of coordinates and the functional determinant of above. By similar techniques as above and using $\lambda_1 + \lambda_2 + r = -g$ we get

$$\begin{aligned} c(x, y, t) &= f \int_0^t e^{gs} \delta(x - \bar{x}(s)) \delta(y - \bar{y}(s)) (N - m(s)) ds, \\ \bar{x}(s) &:= x(0, u(s), s), \\ \bar{y}(s) &:= y(0, u(s), s), \end{aligned} \quad (2.26)$$

and finally

$$\Psi(x, y, t) = c(x, y, t) e^{rt} + \Psi_0(x, y) e^{rt}. \quad (2.27)$$

We recalculate the total number of attached heads to be:

$$\begin{aligned} m(t) &= \iint \Psi(\xi, v, t) d\xi dv \\ &= \iint e^{t(\lambda_1 + \lambda_2)} (c(x, y, t) e^{rt} + \Psi_0(x, y) e^{rt}) dx dy \\ &= m(t) - m_0 e^{-gt} + m_0 e^{-gt} = m(t) \end{aligned}$$

The calculations were done analogously to the stationary case. In its weak formulation the solution takes the form:

$$\begin{aligned} &\langle \Psi(\xi, v, t), \phi(\xi, v) \rangle \\ &= \iint \Psi_0(x(\xi, v, t), y(\xi, v, t)) e^{rt} \phi(\xi, v) d\xi dv \\ &\quad + \iint c(x(\xi, v, t), y(\xi, v, t), t) e^{rt} \phi(\xi, v) d\xi dv \\ &= e^{-gt} \iint \Psi_0(x, y) \phi(\xi(x, y, t), v(x, y, t)) dx dy \\ &\quad + e^{-gt} \iint c(x, y, t) \phi(\xi(x, y, t), v(x, y, t)) dx dy \end{aligned} \quad (2.28)$$

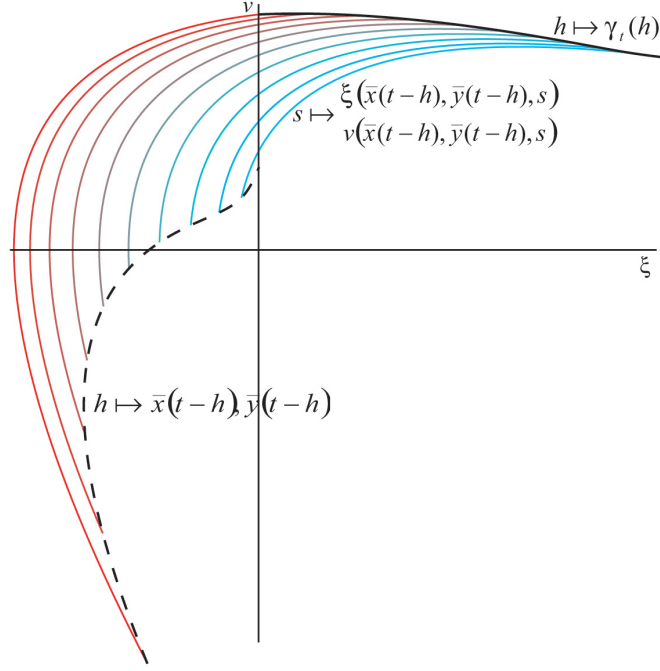
We will take a closer look at the second integral:

$$\begin{aligned} &\langle c(\xi, v, t) e^{rt}, \phi(\xi, v) \rangle \\ &= f e^{-gt} \int_0^t (N - m(s)) e^{gs} \phi(\xi(\bar{x}(s), \bar{y}(s), t), v(\bar{x}(s), \bar{y}(s), t)) ds \\ &= f \int_0^t (N - m(t-h)) e^{-gh} \phi(\xi(\bar{x}(t-h), \bar{y}(t-h), t), v(\bar{x}(t-h), \bar{y}(t-h), t)) dh \\ &= f \int_0^t (N - m(t-h)) e^{-gh} \phi(\gamma_t(h)) dh \end{aligned} \quad (2.29)$$

with

$$\begin{aligned} \gamma_t(h) &: [0, t] \rightarrow R^2 \\ h &\mapsto (\xi(\bar{x}(t-h), \bar{y}(t-h), t), v(\bar{x}(t-h), \bar{y}(t-h), t))) \end{aligned} \quad (2.30)$$

We see that this part of the solution is concentrated on the curve γ_t . For better understanding, we follow the path of a myosin head and pick a time $0 < k < t$. The deltas in the source term guarantee that at that time this head became attached at $(0, u(k))$. The expressions $\bar{x}(k) = x(0, u(k), k)$


 Figure 2.3: $\gamma_t(h)$ and its defining curves

and $\bar{y}(k) = y(0, u(k), k)$ describe where the corresponding characteristic must have been at time 0. Using this starting point and waiting until time t brings us to where that particular head was transported to in the (ξ, v) plane, i.e. to: $(\xi(\bar{x}(k), \bar{y}(k), t), v(\bar{x}(k), \bar{y}(k), t))$. To finally get γ_t we simply set $h = t - k$. We see now that $\gamma_t(h)$ is a curve that starts at $h = 0$ in $(0, u(t))$ and stretches until $\gamma_t(t) = (\xi(0, u_0, t), v(0, u_0, t))$.

Figure 2.3 shows how γ_t is defined. In this graph parameters were used that resulted in $\bar{u} > 0$. We see that the curve $\gamma_t(h)$ forms the support of the solution at time t .

2.4.2 Longtime Behavior

We want to take $t \rightarrow \infty$ in (2.28).

Before looking at the integrals themselves we first need to determine the (pointwise) limit $\lim_{t \rightarrow \infty} \gamma_t(h)$.

Using (2.24) and (2.25) we can write:

$$\begin{aligned} \gamma_t(h) &= e^{At} \left[e^{-A(t-h)} \begin{pmatrix} 0 \\ u(t-h) \end{pmatrix} - C(t-h) \right] + e^{At} C(t) \\ &= e^{Ah} \begin{pmatrix} 0 \\ u(t-h) \end{pmatrix} + e^{At} (C(t) - C(t-h)) \end{aligned} \quad (2.31)$$

We claim that its limit is precisely the stationary characteristic on which the stationary solution is concentrated on. Using (2.19) and (2.20) we can write it as:

$$\gamma_\infty(h) := e^{Ah} \begin{pmatrix} 0 \\ \bar{u} \end{pmatrix} + e^{Ah} \bar{C}(h) \quad (2.32)$$

Convergence in the first part follows from $\lim_{t \rightarrow \infty} u(t) = \bar{u}$.

For the second part we use two results which stem from the fact that the matrix exponential inherits many properties from its 1D version. Let the matrix E be invertible. Further let $B(s)$ be any vector which converges component wise to \bar{B} for $s \rightarrow \infty$. We claim that:

$$\lim_{t \rightarrow \infty} e^{Et} \int_0^{t-h} e^{-Es} B(s) ds = -E^{-1} e^{Eh} \bar{B} \quad (2.33a)$$

$$\int_a^b e^{Es} ds = E^{-1} (e^{Eb} - e^{Ea}) \quad (2.33b)$$

The proofs can be found in section 2.6.2.

With these two facts, the pointwise convergence of γ_t , (2.31), is straightforward: We set $B(s) := (0, Inh(s))$ and $E := A$ and using (2.33a) and $\bar{B} = (0, Inh)$ we get:

$$\begin{aligned} e^{At} (C(t) - C(t-h)) &= e^{At} \int_0^t e^{-As} \begin{pmatrix} 0 \\ Inh(s) \end{pmatrix} ds - e^{At} \int_0^{t-h} e^{-As} \begin{pmatrix} 0 \\ Inh(s) \end{pmatrix} ds \\ &\rightarrow -A^{-1} \begin{pmatrix} 0 \\ Inh \end{pmatrix} + A^{-1} e^{Ah} \begin{pmatrix} 0 \\ Inh \end{pmatrix} \end{aligned}$$

To check that this corresponds to the second part in (2.32) we use the claim in (2.33b) by setting $E := -A$ and noting that A^{-1} and e^{Ah} commute.

Together we have shown that $\lim_{t \rightarrow \infty} \gamma_t(h) = \gamma_\infty(h)$ for each fixed h . Fig. 2.4 shows how $\gamma_t(h)$ gets closer to the stationary characteristic for increasing t . The $\gamma_t(h)$ shown in Fig. 2.3 corresponds to $\gamma_{t_5}(h)$ in this figure.

Now we are ready to take t to infinity in the full solution. Let $\epsilon > 0$.

First we need specify what kind of test functions we want to work with. Let $\phi(\xi, v) \in C_B(\mathbb{R}^2) := C(\mathbb{R}^2) \cap L^\infty(\mathbb{R}^2)$. Further we define $M := \sup_{\mathbb{R}^2} |\phi|$.

We call the two integrals in (2.28) I_1 and I_2 (with I_2 already rewritten as explained in (2.29)):

$$\begin{aligned} I_1 &:= e^{-gt} \iint \Psi_0(x, y) \phi(\xi(x, y, t), v(x, y, t)) dx dy \\ I_2 &:= f \int_0^t (N - m(t-h)) e^{-gh} \phi(\gamma_t(h)) dh \end{aligned}$$

We start with the first integral and find that due to ϕ being bounded:

$$|I_1| \leq e^{-gt} M \iint \Psi_0(x, y) dx dy \leq e^{-gt} M m_0$$

This converges to 0 for $t \rightarrow \infty$. We can therefore find a $T_1 > 0$ such that

$$|I_1| \leq \frac{\epsilon}{3} \quad (2.34)$$

for $t > T_1$.

We see that the initial distribution Ψ_0 doesn't contribute to the long term behavior. This is due to the fact that we assume a positive detachment rate g of the heads. After the eventual detachment the myosin heads can only attach again at the point $(0, u(t))$ and therefore the influence of the initial head distribution decreases with time.

We now claim that the rest converges to the stationary solution defined in (2.22) which takes the following weak form:

$$\begin{aligned}
 I_\infty &:= \langle \bar{\Psi}, \phi \rangle = f(N - \bar{m}) \int_0^{2\Pi} \int_{-\infty}^{\infty} \delta(w) H(h) e^{-gh} \phi(\xi(w, h), v(w, h)) dh dw \\
 &= f(N - \bar{m}) \int_0^{\infty} e^{-gh} \phi(\xi(0, h), v(0, h)) dh \\
 &= f(N - \bar{m}) \int_0^{\infty} e^{-gh} \phi(\gamma_\infty(h)) dh
 \end{aligned} \tag{2.35}$$

To estimate the difference between I_2 and I_∞ we split both integrals at a point $\tau \in (0, t)$ and get:

$$\begin{aligned}
 |I_2 - I_\infty| &= \left| f \int_0^\tau (N - m(t-h)) e^{-gh} \phi(\gamma_t(h)) dh - f(N - \bar{m}) \int_0^\tau e^{-gh} \phi(\gamma_\infty(h)) \right. \\
 &\quad \left. + f \int_\tau^t (N - m(t-h)) e^{-gh} \phi(\gamma_t(h)) dh - f(N - \bar{m}) \int_\tau^\infty e^{-gh} \phi(\gamma_\infty(h)) \right|
 \end{aligned}$$

We call the first difference A_1 and second one A_2 and estimate them separately.

$$\begin{aligned}
 |A_2| &\leq \left| f \int_\tau^t (N - m(t-h)) e^{-gh} \phi(\gamma_t(h)) dh \right| + (N - \bar{m}) \left| f \int_\tau^\infty e^{-gh} \phi(\gamma_\infty(h)) dh \right| \\
 &\leq M \max\{N - m_0, N - \bar{m}\} f \int_\tau^t e^{-gh} dh + M(N - \bar{m}) f \int_\tau^\infty e^{-gh} dh \\
 &\leq M \max\{N - m_0, N - \bar{m}\} \frac{f}{g} (e^{-g\tau} - e^{-gt}) + M(N - \bar{m}) \frac{f}{g} e^{-g\tau} \\
 &\leq 2M \max\{N - m_0, N - \bar{m}\} \frac{f}{g} e^{-g\tau} \\
 &\leq \frac{\epsilon}{3}
 \end{aligned} \tag{2.36}$$

The first line uses the triangle inequality, the second that ϕ is bounded and the fact that $m(t)$ takes its minimum either at m_0 or at \bar{m} , both smaller than N . In the fourth inequality we simply drop the negative term. We can make the last inequality true by choosing τ large enough.

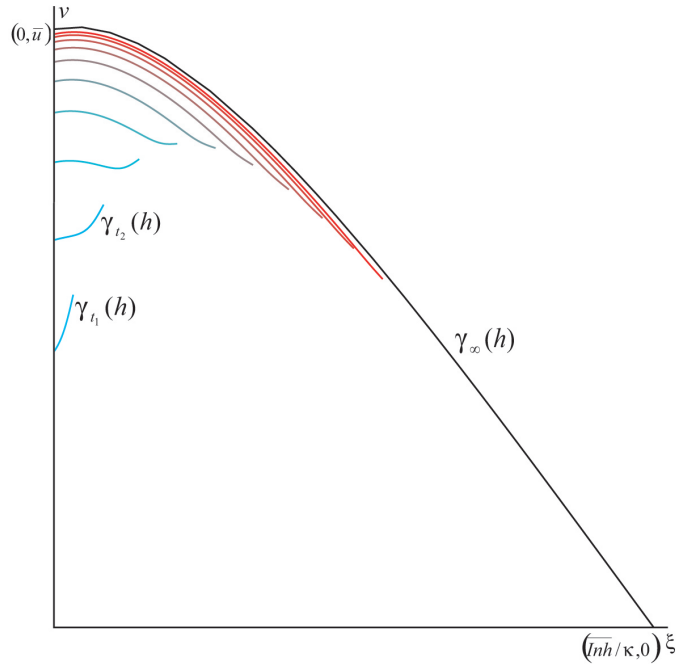
For A_1 we use the fact that $\lim_{t \rightarrow \infty} m(t) = \bar{m}$ and the pointwise convergence of $\gamma_t(h)$ shown above. Together with the continuity of ϕ that tells us that for the τ chosen above we can find a $T_2 < 0$ such that $\forall t > T_2$:

$$|A_1| \leq f \int_0^\tau e^{-gh} |((N - m(t-h)) \phi(\gamma_t(h))) - ((N - \bar{m}) \phi(\gamma_\infty(h)))| dh \leq \frac{\epsilon}{3} \tag{2.37}$$

Finally we put (2.34), (2.36) and (2.37) together. Let $\bar{T} := \max\{T_1, T_2\}$. Then we have for all $t > \bar{T}$:

$$\begin{aligned}
 |I_1 + I_2 - I_\infty| &\leq |I_1| + |I_2 - I_\infty| \\
 &\leq |I_1| + |A_1| + |A_2| \\
 &\leq \frac{\epsilon}{3} + \frac{\epsilon}{3} + \frac{\epsilon}{3} = \epsilon
 \end{aligned}$$

This makes the convergence of the full solution exact. We summarize this result in the following

Figure 2.4: Some $\gamma_{t_i}(h)$ and its limiting curve for $t \rightarrow \infty$

Theorem: Let $\gamma_t(h)$ and $\gamma_\infty(h)$ be defined as in (2.30) and (2.32) respectively. Let $\Psi_0(\xi, v)$ be defined such that its moments m_0 , u_0 and σ_0 (calculated as in (2.1)) exist with $0 < m_0 \leq N$. Let further \bar{m} , \bar{u} and $\bar{\sigma}$ be defined as in (2.9).

Then we have tight convergence on the set of non-negative, bounded Radon measures \mathcal{M}_1^+ of Ψ , the solution of equation (2.23) (as defined in (2.28)) to $\bar{\Psi}$, the solution of the stationary equation (2.16) (as defined in (2.35)) i.e. for all $\phi \in C_B(\mathbb{R}^2)$ we have:

$$\begin{aligned} \langle \Psi, \phi \rangle &= \\ e^{-gt} \iint \Psi_0(x, y) \phi(\xi(x, y, t), v(x, y, t)) dx dy &+ f \int_0^t (N - m(t-h)) e^{-gh} \phi(\gamma_t(h)) dh \\ \xrightarrow{t \rightarrow \infty} f(N - \bar{m}) \int_0^\infty e^{-gh} \phi(\gamma_\infty(h)) dh &= \langle \bar{\Psi}, \phi \rangle \end{aligned}$$

2.5 Interpretation

The characteristics describe the path of individual myosin heads in the phase space (ξ, v) under the influence of the forces described. They all tend to the position

$$(\xi, v) = \left(\frac{In\bar{h}}{\kappa}, 0 \right) = \left(\bar{u} \left(\frac{1}{g} + \frac{1}{\kappa} \left(\eta + \frac{1}{T} \right) \right), 0 \right)$$

If the external force equals the stall force (i.e. the force such that $\bar{u} = 0$), $F_{stall} = \kappa \xi_0 \bar{m}$ we get $\frac{In\bar{h}}{\kappa} = 0$, so the heads just stay at their attachment position and there is no movement.

If on the other hand $F = 0$, only the friction forces $\frac{\bar{u}-v}{T}$ and $-\eta v$ and the spring force $\kappa(\xi_0 - \xi)$

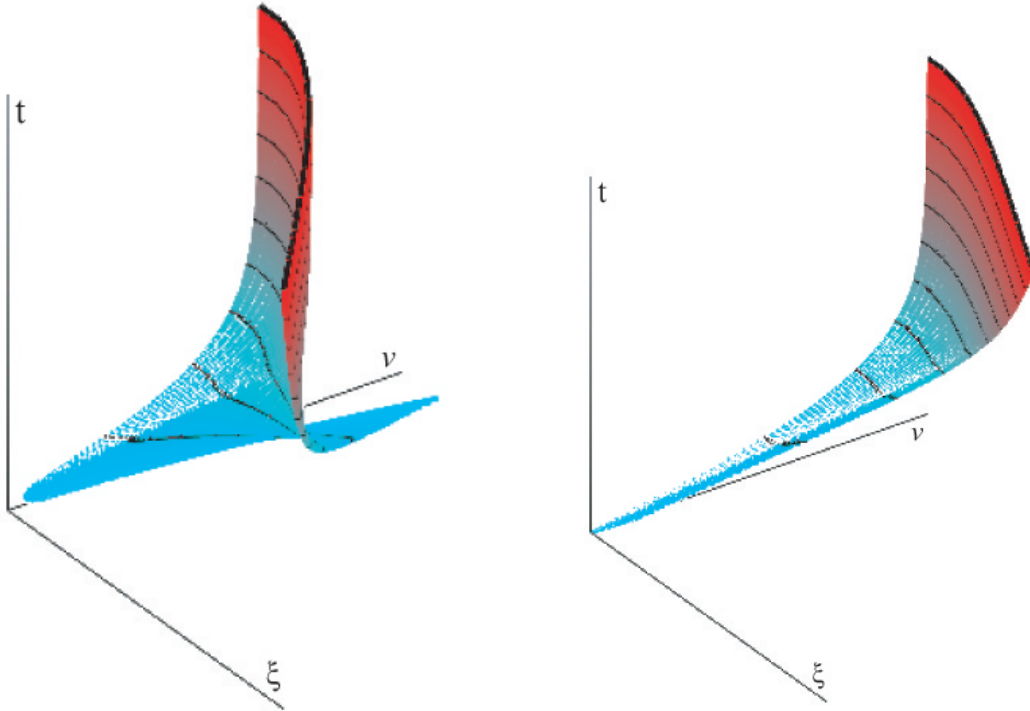


Figure 2.5: The support of the solution for two different parameter sets. The right picture uses the same parameters as figure 2.3.

are active, resulting in an equilibrium position ξ of $\xi_0 \left(1 + \frac{g}{T(\kappa + g\eta)}\right) > \xi_0$, which means that the heads are dragged past their equilibrium position by the bundle movement.

In the full equation we have an initial distribution Ψ_0 which puts heads at any point in the phase space. However, because we assume a positive detachment rate $g > 0$ the heads move along their characteristics, but will eventually detach and only enter again at $(0, u(t))$. As $\lim_{t \rightarrow \infty} u(t) = \bar{u}$ it seems reasonable that for large times we observe a concentration of mass on the (stationary) characteristic going through $(0, \bar{u})$, but only on the part leading from $(0, \bar{u})$ to $\left(\frac{T\bar{h}}{\kappa}, 0\right)$. The exact amount of heads decreased exponentially along the characteristic (because of the factor $e^{-g t}$), which is precisely the situation described by the stationary solution. Figure 2.5 shows a 3D Plot of the support of the full solution. The z-direction represents the time. The resulting surface can have very different shapes, depending on the chosen parameters. The right picture corresponds to the parameters which were also used for 2.3.

2.6 Appendix

2.6.1 Where to define Initial Conditions

The Case $\lambda_1 \neq \lambda_2$

The system can be diagonalized. To transform the system into its canonical shape, we will

use the matrix Q , which is the change of basis matrix for diagonalizing A ($Q J Q^{-1} = A$). In case of real eigenvalues, also Q will have real entries. In the case of complex eigenvalues $\lambda_{1,2} = a \pm i b$ we use the real Jordan canonical form and the corresponding real change of basis matrix for J and Q respectively:

$$\begin{pmatrix} \hat{\xi} \\ \hat{v} \end{pmatrix} := Q^{-1} \begin{pmatrix} \xi \\ v \end{pmatrix} + S \quad (2.38)$$

with $S := -Q^{-1} \begin{pmatrix} \overline{Inh} \\ \kappa \\ 0 \end{pmatrix}$ and $Q^{-1} := \begin{pmatrix} 1 & -\frac{1}{\lambda_2} \\ 1 & -\frac{1}{\lambda_1} \end{pmatrix}$ or $Q^{-1} := \begin{pmatrix} 0 & 1 \\ -\frac{\kappa}{a} & \frac{1}{b} \end{pmatrix}$ for the real and complex case respectively.

The translation S just maps the limit point $\left(\frac{\overline{Inh}}{\kappa}, 0\right)$ to the origin. The new canonical system now corresponds to the ODE:

$$\begin{pmatrix} \dot{\hat{\xi}} \\ \dot{\hat{v}} \end{pmatrix} = J \begin{pmatrix} \hat{\xi} \\ \hat{v} \end{pmatrix}$$

Now we define initial conditions for the new system on a circle:

$$\begin{pmatrix} \hat{\xi}_0(w) \\ \hat{v}_0(w) \end{pmatrix} := (R \cos(w_u - w), R \sin(w_u - w))$$

R and w_u are constants that can still be chosen. Next we transform them back into the old system using (2.38). We get:

$$\begin{pmatrix} \xi_0(w) \\ v_0(w) \end{pmatrix} = Q \left[\begin{pmatrix} \hat{\xi}_0(w) \\ \hat{v}_0(w) \end{pmatrix} - S \right]$$

which equals

$$\begin{pmatrix} \frac{1}{\lambda_1 - \lambda_2} (\lambda_1 R \sin(w_u - w) - \lambda_2 R \cos(w_u - w)) + \frac{\overline{Inh}}{\kappa} \\ \frac{\kappa R}{\lambda_1 - \lambda_2} (\sin(w_u - w) - \cos(w_u - w)) \end{pmatrix} \text{ and} \\ \begin{pmatrix} \frac{1}{\kappa} (a R \cos(w_u - w) - b R \sin(w_u - w) + Inh) \\ R \cos(w_u - w) \end{pmatrix}$$

for the real and complex case respectively.

As this is a linear transformation, the circle is transformed into an ellipse, which is also depicted in Figure 2.2. These initial conditions we put into the system (2.19). We will later see that the δs in the equation have the effect that the characteristic starting at $(0, \bar{u})$ plays a special role. To account for that and make future calculations easier, we choose R and w_u is such a way and $(\xi_0(0), v_0(0)) = (0, \bar{u})$. Therefore we see that:

$$(\xi(0, 0), v(0, 0)) = (0, \bar{u})$$

which will be practical later on.

Now we need to check that with this choice of initial conditions the parameter change $(w, s) \rightarrow (\xi, v)$ is bijective we calculate the determinant of the Jacobian

$$\begin{pmatrix} \partial_w \xi & \partial_s \xi \\ \partial_w v & \partial_s v \end{pmatrix}$$

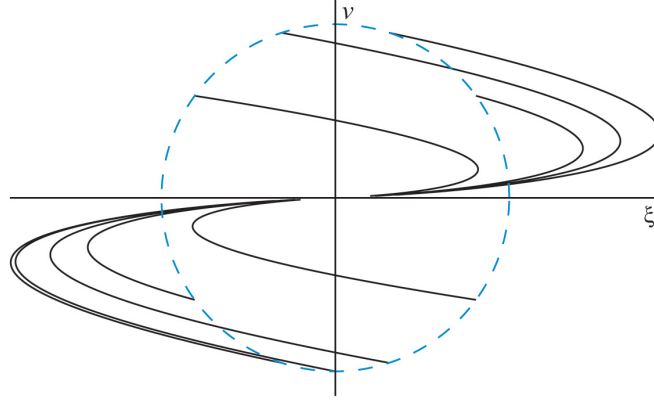


Figure 2.6: The characteristics of the transformed system for the case $\lambda_1 = \lambda_2$.

to be:

$$J(w, s) := \frac{R^2 \kappa e^{s(\lambda_1 + \lambda_2)}}{\lambda_1 - \lambda_2} (\lambda_1 \cos^2(w_u - w) + \lambda_2 \sin^2(w_u - w)) > 0$$

for the real case and

$$J(w, s) := -\frac{R^2 a b e^{2as}}{\kappa} > 0$$

in the complex case. Both are always positive. Finally we define $J_0 := J(0, 0)$.

The Case $\lambda_1 = \lambda_2$

If $\kappa = \frac{1}{4}(\eta + \frac{1}{T})^2$ the Matrix A has a twofold eigenvalue $\lambda_0 := -\sqrt{\kappa}$ and cannot be diagonalized. Instead we look at the system described by its Jordanform by setting Q^{-1} and S from above to be

$$\begin{pmatrix} 0 & -\frac{1}{\lambda_0^2} \\ 1 & -\frac{1}{\lambda_0} \end{pmatrix} \text{ and } \begin{pmatrix} 0 & \\ -\frac{I\eta h}{\kappa} & \end{pmatrix} \text{ respectively:}$$

The solutions of the transformed system take the following shape:

$$\begin{pmatrix} \hat{\xi}(w, s) \\ \hat{v}(w, s) \end{pmatrix} = \begin{pmatrix} \hat{\xi}_0(w) e^{\lambda_0 s} + t \hat{v}(w) e^{\lambda_0 s} \\ \hat{v}_0(w) e^{\lambda_0 s} \end{pmatrix}$$

Figure 2.6 shows the characteristics of the transformed system. From the figure it becomes quite clear why it cannot work to define the starting points to be on a circle. Instead we chose an ellipse with its center at the origin, parallel to the w axis and with axes lengths L and R . As a condition that characteristics at their starting points cannot be tangential to the ellipse one gets: $L \geq -\frac{R}{2\lambda_0}$ and therefore we choose to define $L := -\frac{R}{\lambda_0}$. Again we define R and w_u in such a way that $(-\frac{R}{\lambda_0} \cos(w_u), R \sin(w_u))$ mapped back to the original system equals $(0, \bar{u})$ (see above).

We then get:

$$\begin{aligned}\xi(w, s) &:= e^{\lambda_0 s} (R \sin(w_u - w) + R \cos(w_u - w) - s \lambda_0 R \sin(w_u - w)) + \frac{\overline{Inh}}{\kappa} \\ v(w, s) &:= e^{\lambda_0 s} \lambda_0 R (\cos(w_u - w) - s \lambda_0 \sin(w_u - w))\end{aligned}\quad (2.39)$$

And

$$J(w, s) := R^2 \kappa e^{2s\lambda_0} (1 - \cos(w) \sin(w)) > 0$$

2.6.2 Properties of the Matrix Exponential

It is sufficient to show the two results claimed in 2.33a and 2.33b for a Jordan-block. W.l.o.g. we set $h = 0$ in 2.33a. Therefore we want to show:

$$\lim_{t \rightarrow \infty} e^{Jt} \int_0^t e^{-Js} B(s) ds = -J^{-1} \overline{B} \quad (2.40a)$$

$$\int_a^b e^{Js} ds = J^{-1} (e^{Jb} - e^{Ja}) \quad (2.40b)$$

with

$$J = \begin{pmatrix} \alpha & 1 & 0 & \cdots & 0 \\ 0 & \alpha & 1 & \cdots & 0 \\ \vdots & \ddots & \ddots & \ddots & \vdots \\ \vdots & & & \ddots & \alpha & 1 \\ 0 & \cdots & \cdots & 0 & \alpha \end{pmatrix}$$

For the first part we note that:

$$\begin{aligned}(\exp Jt)_{ij} &= \begin{cases} 0 & j < i \\ e^{\alpha t} \frac{t^{j-i}}{(j-i)!} & \text{else} \end{cases} \\ D_i &:= \sum_{k=1}^n (\exp(-Js))_{ik} B(s)_k = \sum_{k=i}^n (\exp(-Js))_{ik} B(s)_k \\ C_i &:= \int_a^t D_i \\ E_i &:= (\exp Jt C)_i = \sum_{l=1}^n (\exp(Jt)_{il}) C_l = \sum_{l=i}^n (\exp(Jt)_{il}) C_l \\ &= \sum_{l=i}^n \sum_{k=l}^n \frac{(-1)^{k-l}}{(k-l)!(l-i)!} e^{\alpha t} t^{l-i} \int_a^t e^{-\alpha s} s^{k-l} B(s)_k ds\end{aligned}$$

We define the argument of the double sum as $A(i, k, l)$ and using the rule of de'Hospital, we see that it has the same limit as $-\frac{1}{\alpha} \left[A(i+1, k, l) + \frac{(-1)^{k-i}}{(k-l)!(l-i)!} t^{k-i} \overline{B}_k \right]$. Next we apply J from the right to the limit to find:

$$(JE)_i = \sum_{m=1}^n J_{im} E_m = \alpha E_i + E_{i+1}$$

$$\begin{aligned}
 &= \alpha \sum_{l=i}^n \sum_{k=l}^n A(i, k, l) + \sum_{l=i+1}^n \sum_{k=l}^n A(i+1, k, l) \\
 &= \alpha A(i, k, i) - \left[\sum_{l=i+1}^n \sum_{k=l}^n A(i+1, k, l) + \frac{(-1)^{k-l}}{(k-l)!(l-i)!} t^{k-i} \bar{B}_k \right] \\
 &\quad + \sum_{l=i+1}^n \sum_{k=l}^n A(i+1, k, l) \\
 &= - \sum_{l=i}^n \sum_{k=l}^n \frac{(-1)^{k-l}}{(k-l)!(l-i)!} t^{k-i} \bar{B}_k = - \sum_{k=i}^n t^{k-i} \bar{B}_k \sum_{l=i}^k \frac{(-1)^{k-l}}{(k-l)!(l-i)!} \\
 &= - \sum_{k=i}^n t^{k-i} \bar{B}_k \frac{1}{(k-i)!} \sum_0^{k-i} \binom{k-i}{l} (-1)^{k-i-l} = - \sum_{k=i}^n t^{k-i} \bar{B}_k \frac{1}{(k-i)!} (1-1)^{k-i} \\
 &= - \bar{B}_i
 \end{aligned}$$

This finishes the proof of the first part of 2.40a.

In a similar way we proof the second part.

We need to show that:

$$\begin{aligned}
 \int_a^b e^{Js} ds &= J^{-1} (e^{Jb} - e^{Ja}) \iff \\
 J \int_a^b e^{Js} ds &= e^{Jb} - e^{Ja} \iff JI = K
 \end{aligned}$$

with I and K defined as the integral and the right hand side of the equation respectively.

$$(K)_{ij} = \begin{cases} 0 & j < i \\ e^{\alpha b} \frac{b^{j-i}}{(j-i)!} - e^{\alpha a} \frac{a^{j-i}}{(j-i)!} & \text{else} \end{cases}$$

To find an expression for I we need to integrate

$$(e^{Js})_{ij} = \begin{cases} 0 & j < i \\ e^{\alpha s} \frac{s^{j-i}}{(j-i)!} & \text{else} \end{cases}$$

Using integration by parts we find that:

$$B_k := \frac{1}{k!} \int_a^b e^{\alpha s} s^k ds = \frac{1}{\alpha} \left[\frac{1}{k!} (e^{\alpha b} b^k - e^{\alpha a} a^k) - B_{k-1} \right]$$

We see that $(I_{ij}) = B_{j-i}$ for $j \geq i$ and finish by calculating:

$$\begin{aligned}
 (JI)_{ij} &= \sum_{k=1}^n J_{ik} I_{kj} = J_{ii} I_{ij} + J_{i+1} I_{i+1j} = \alpha B_{j-i} + B_{j-i-1} \\
 &= \frac{1}{(j-i)!} (e^{\alpha b} b^{j-i} - e^{\alpha a} a^{j-i}) - B_{j-i-1} + B_{j-i-1} \\
 &= (K)_{ij}
 \end{aligned}$$

3 Application to Keratocyte Movement

3.1 Introduction

As discussed in Chapter 1, Section 1.6 fish keratocytes are useful model cells for studying cell movement. In this chapter we want to model the effect of actin-myosin interactions on the movement of these cells. To do that we will also include some of the results of Chapter 2.

A very useful property of keratocytes is that, if treated with certain drugs (e.g. *staurosporine*) and/or temperature shifts, they start losing parts of their lamellipodium. These parts are called *cytoplasts* (because they contain mainly cytoplasm) and surprisingly exhibit the same moving behavior as the original cells: They can also be stationary and circular or half-moon shaped and moving. This fact indicates that the fragments contain all that is necessary for movement. Additionally they do not have any nucleus and other cell organelles which makes them easier to examine, e.g. under the electron microscope, where a cell body can be interfering. Figure 3.1 shows still attached cytoplasm and also a free moving cytoplast.

This simplified system was modeled in Oelz and Schmeiser [2010c]. There the following effects were included:

- bending of actin filaments
- twisting and stretching of cross-linking proteins between actin filaments
- stretching of the plasma membrane
- formation and breakage of adhesions, with which the cell attaches to the substrate

Here we additionally want to introduce myosin filaments that act on actin (see Chapter 1 for background information on actin and myosin). The modeling assumptions, model description, non-dimensionalization and derivation of the Euler-Lagrange equation of the original model are

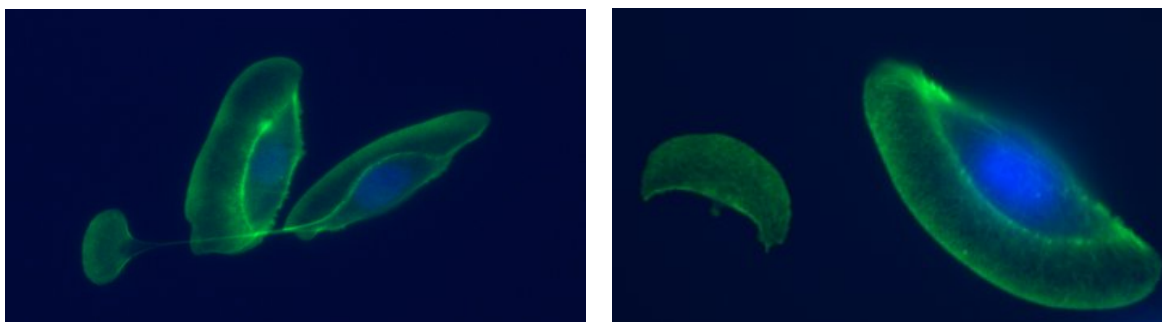


Figure 3.1: The left picture shows two keratocytes with one losing cytoplasm. The right picture shows a full keratocyte and one freely moving cytoplast. Actin is labeled green, the nucleus blue. Source: self made

described in the following part. How the new myosin terms are incorporated will be described in the second part.

3.2 Lamellipodium Modeling

This part closely follows Oelz and Schmeiser [2010c].

The original model has as a central feature an age-structured production and decay of cross-links and adhesions. It starts with a discrete description of the actin filaments to then perform a homogenization limit, letting the number of filaments tend to infinity based on the assumption that their density within the lamellipodium is high. We will use the homogenized model as a starting point.

3.2.1 Assumptions and General Modeling

The following seven assumptions are made:

A1: *The lamellipodium is two dimensional and has the topology of a ring, i.e. it lies between two closed curves.*

A2: *All actin filaments belong to two families, called clockwise and anti-clockwise. Filaments of the same family do not cross each other. Crossing of clockwise and anti-clockwise filaments are transversal. All barbed ends touch the leading edge of the lamellipodium, i.e. the outer curve of the previous assumption. Filaments are inextensible.*

A3: *Filaments polymerize at the barbed ends with given polymerization speed. Depolymerization at the pointed ends is a stochastic process with prescribed distribution.*

A4: *A cross-link is a connection between a material point on a clockwise and a material point on an anti-clockwise filament. Cross-links can be created spontaneously at the crossing between two filaments and they can also break. Creation and breaking are stochastic processes. There exists at most one cross-link for any pair of filaments at any time.*

A5: *An adhesion is a connection between a material point on a filament and a point on the substrate via a transmembrane linkage. Adhesions can be created spontaneously and they can also break. Creation and breaking are stochastic processes. The number of adhesions per filament length is restricted.*

A6: *The position of the filaments is determined by a quasi-stationary balance of elastic forces resulting from bending the filaments, stretching and twisting the cross-links, stretching the adhesions, and stretching the cell membrane around the leading edge.*

A7: *The cell membrane simulates a rubber band stretched around the barbed ends of the filaments.*

The Filaments

Figure 3.2 shows the orientation and position of the both filament groups within the lamellipodium.

The clockwise filaments are labeled with $+$, the anti-clockwise with $-$ and their positions at time t are described by $F^+(t, \alpha^+, s)$ and $F^-(t, \alpha^-, s)$. Here $\alpha^\pm \in [-\pi, \pi)$ labels the different filaments and $s \in [-L, 0]$ represents the arc length, i.e. the position on one filament. L describes the maximum length of a filament and the positions $s = 0$ and $s = -L$ refer to the barbed and pointed end respectively. Together we get continuous functions F^\pm with:

$$F^\pm : [0, \infty) \times B \rightarrow \mathbb{R}^2 \quad \text{with} \quad B := [-\pi, \pi] \times [-L, 0]$$

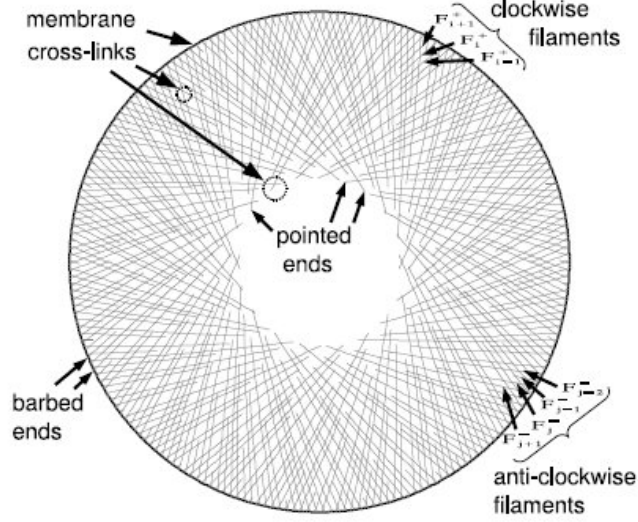


Figure 3.2: The arrangement and labeling of filaments in the lamellipodium. Source: Oelz and Schmeiser [2010c]

The fact that two filaments of the same family do not cross (**A2**) implies that F^\pm is one-to-one. The lengths of the filaments are random variables with given distributions (**A3**):

$$\eta^\pm : [0, \infty) \times B \rightarrow [0, 1]$$

with the deterministic interpretation as the expected fraction of filaments in each index element $d\alpha$, whose length at time t is bigger than $-s$.

Next we need to specify where filaments cross, because here cross-links and myosin filaments can form. We construct a set of index pairs:

$$\mathcal{C}(t) = \{(\alpha^+, \alpha^-) \in [0, 2\pi)^2 : \exists s^\pm(t, \alpha^+, \alpha^-) \text{ such that} \\ F^+(t, \alpha^+, s^+(t, \alpha^+, \alpha^-)) = F^-(t, \alpha^-, s^-(t, \alpha^+, \alpha^-))\}$$

We assumed that two given filaments can cross at most at one point (**A4**), therefore for each $(\alpha^+, \alpha^-) \in \mathcal{C}(t)$ there is only one $s^\pm(t, \alpha^+, \alpha^-)$. If we define

$$B^\pm(t) := \{(\alpha^\pm, s^\pm(t, \alpha^+, \alpha^-)) : (\alpha^+, \alpha^-) \in \mathcal{C}(t)\} \subset B$$

the maps $(\alpha^+, \alpha^-) \mapsto (\alpha^\pm, s^\pm(t, \alpha^+, \alpha^-))$ from $\mathcal{C}(t)$ to $B^\pm(t)$ are invertible.

We define the angle between crossing filaments by:

$$\phi(t, \alpha^+, \alpha^-) = \arccos [\partial_s F^+(t, \alpha^+, s^+(t, \alpha^+, \alpha^-)) \cdot \partial_s F^-(t, \alpha^-, s^-(t, \alpha^+, \alpha^-))]$$

Cross-links

Cross-links form between two actin monomers and stay attached to them (**A4**). If the monomers move away from each other, the cross-link is stretched, against which it shows resistance. Additionally it is assumed that the cross-link prefers a certain angle ϕ_0 between the two filaments which leads to twisting forces, if that angle is changed.

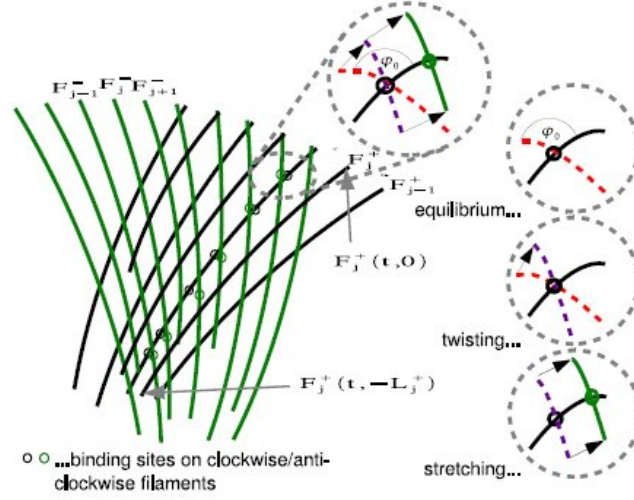


Figure 3.3: Cross-links and associated forces. Source: Oelz and Schmeiser [2010c]

Because of the addition of new actin monomers at the barbed end, material points on the filaments (i.e. actin monomers) move from the barbed to the pointed end with polymerization speed $v^\pm(t, \alpha)$ (**A3**).

Therefore the material point of a cross-link of age a has the following s -label:

$$s_a^+(t, \alpha^+, \alpha^-) := s^+(t - a, \alpha^+, \alpha^-) - \int_{t-a}^t v^+(\tilde{t}, \alpha^+) d\tilde{t} \quad (3.1)$$

$$s_a^-(t, \alpha^+, \alpha^-) := s^-(t - a, \alpha^+, \alpha^-) - \int_{t-a}^t v^-(\tilde{t}, \alpha^-) d\tilde{t}$$

Figure 3.3 shows a detailed view of the forces caused by cross-links which can be described by a stretching force S and a twisting force T calculated as follows:

$$S(t, a, \alpha^+, \alpha^-) = F^+(t, \alpha^+, s_a^+(t, \alpha^+, \alpha^-)) - F^-(t, \alpha^+, s_a^-(t, \alpha^+, \alpha^-)) \quad (3.2)$$

$$T(t, a, \alpha^+, \alpha^-) = \phi_a(t, \alpha^+, \alpha^-) - \phi_0$$

with

$$\phi_a(t, \alpha^+, \alpha^-) = \arccos [\partial_s F^+(t, \alpha^+, s_a^+(t, \alpha^+, \alpha^-)) \cdot \partial_s F^-(t, \alpha^-, s_a^-(t, \alpha^+, \alpha^-))]$$

We define

$$T_0(t, \alpha^+, \alpha^-) = T(t, 0, \alpha^+, \alpha^-). \quad (3.3)$$

For the expected cross-link density $\rho(t, a, \alpha^+, \alpha^-)$ with $(\alpha^+, \alpha^-) \in \mathcal{C}(t - a)$ we can derive a transport equation with a breaking rate ζ that depends on how stretched and twisted the cross-link is. Further we need a creation rate $\beta(T_0)$ dependent on the angle at the time of formation and boundary conditions.

$$\partial_t \rho + \partial_a \rho = -\zeta(S, T) \rho \quad (3.4)$$

$$\begin{aligned}\rho(a=0) &= \beta(T_0) \left(1 - \int_0^\infty \rho da\right) \\ \rho(t, a, \alpha^+, \alpha^-) &= 0 \quad \text{for } (\alpha^+, \alpha^-) \in \partial\mathcal{C}(t-a)_+ \\ \rho(t=0) &= \rho^I\end{aligned}$$

with $\partial\mathcal{C}(t-a)_+$ denoting the part of the boundary of $\mathcal{C}(t-a)$ where the filaments with labels α^+ and α^- start having a crossing.

If the length distributions of the filaments η^+ and η^- are taken into account, one can define an effective cross-link density and an associated transport equation:

$$\begin{aligned}\rho^{eff}(t, a, \alpha^+, \alpha^-) &= \rho(t, a, \alpha^+, \alpha^-) \eta^+(t, \alpha^+, s_a^+(t, \alpha^+, \alpha^-)) \eta^-(t, \alpha^-, s_a^-(t, \alpha^+, \alpha^-)) \\ \partial_t \rho^{eff} + \partial_a \rho^{eff} &= -\rho^{eff} \left(\zeta(S, T) - \frac{\partial_t \eta^+ - v^+ \partial_s \eta^+}{\eta^+} - \frac{\partial_t \eta^- - v^- \partial_s \eta^-}{\eta^-} \right)\end{aligned}$$

Now we look at the dynamics of

Adhesions

The densities $\rho_{adh}^\pm(t, a, \alpha, s)$ satisfy the following differential equations and boundary conditions (**A5**):

$$\begin{aligned}\partial_t \rho_{adh}^\pm + \partial_a \rho_{adh}^\pm - v^\pm \partial_s \rho_{adh}^\pm &= -\zeta_{adh}(S_{adh}^\pm) \rho_{adh}^\pm \\ \rho_{adh}^\pm(a=0) &= \beta_{adh} \left(\overline{\rho_{adh}} - \int_0^\infty \rho_{adh}^\pm da \right) \\ \rho_{adh}^\pm(s=0) &= 0 \\ \rho_{adh}^\pm(t=0) &= \rho_{adh}^{I\pm}\end{aligned}$$

where $\overline{\rho_{adh}}$ describes the maximal density of adhesions along the filament and

$$S_{adh}^\pm(t, a, \alpha, s) := F^\pm(t, \alpha, a) - F^\pm \left(t - a, \alpha, s + \int_{t-a}^t v^\pm(\tilde{t}, \alpha) d\tilde{t} \right)$$

The Energy Functional

Assumption **A6** tells us that elastic oscillations are neglected because they are assumed to be damped by the cytosol. Further it says the filament positions minimize a potential energy functional consisting of contributions from the described effects:

$$\begin{aligned}U(t) [G^+, G^-] &:= U_{bend}^+(t) [G^+] + U_{bend}^-(t) [G^-] + U_{scl+tcl}(t) [G^+, G^-] \\ &\quad + U_{memb} [G^\pm] + U_{adh}^+(t) [G^+] + U_{adh}^-(t) [G^-]\end{aligned} \quad (3.5)$$

with

$$\begin{aligned}U_{bend}^\pm(t) [G^\pm] &:= \frac{\kappa^B}{2} \int_B |\partial_s^2 G^\pm|^2 \eta^\pm d(\alpha, s) \\ U_{scl+tcl}(t) [G^+, G^-] &:= \int_0^\infty \int_{\mathcal{C}(t-a)} \left(\frac{\kappa^S}{2} |S|^2 + \frac{\kappa^T}{2} T^2 \right) \rho^{eff} d(\alpha^+, \alpha^-) da \\ U_{adh}^\pm(t) [G^\pm] &:= \frac{\kappa^F}{2} \int_B \int_0^\infty \left| G^\pm - F^\pm \left(t - a, \alpha^\pm, s + \int_{t-a}^t v^\pm(\tilde{t}, a) d\tilde{t} \right) \right|^2 \rho_{adh}^\pm \eta^\pm da d(\alpha, s) \\ U_{memb} [G^\pm] &:= \kappa^M \left(\frac{C^+[G^+] + C^-[G^-]}{2} - C_0 \right)_+^2\end{aligned} \quad (3.6)$$

with

$$C^\pm [G^\pm] := \int_{-\pi}^{\pi} |\partial_\alpha G^\pm(t, \alpha, 0)| d\alpha$$

The last contribution U_{memb} takes the resistance of the membrane against stretching into account; C_0 is the equilibrium circumference. U_{bend} describes the effect of bending the actin filaments, $U_{scl+tbl}$ the stretching and twisting forces caused by the cross-links and U_{adh} refers to the adhesions.

Now the positions of the filaments F^\pm at time t are determined by

$$U(t) [F^+(t, \cdot, \cdot), F^-(t, \cdot, \cdot)] = \min U(t) [G^+, G^-]$$

and under the constraints of inextensibility and that all barbed ends touch the leading edge:

$$\begin{aligned} |\partial_s G^+| &= |\partial_s G^-| = 1 \\ \{G^+(t, \alpha, 0) : -\pi \leq \alpha < \pi\} &= \{G^-(t, \alpha, 0) : -\pi \leq \alpha < \pi\} \end{aligned} \quad (3.7)$$

3.2.2 The Limit of instantaneous Cross Link and Adhesion Turnover

To reduce computational costs and because so far macroscopic and microscopic length scales are still mixed, an asymptotic limit will be performed based on the assumption that the average lifetime of an adhesion and cross-link is small. This will also remove the delay problem, that at this point is part of the energy contributions of the adhesions and cross-links (until now the history of the dynamics would have to be kept until the maximum age of cross-links and adhesions).

Non-dimensionalization

To be able to compare smallness of quantities, the equations first need to be non-dimensionalized. We choose the following reference values:

- the typical filament length L for s , F^\pm , S , S_{adh}^\pm and C_0
- v_0 as reference speed for v_\pm
- the typical time an actin monomer spends in a filament L/v_0 for scaling t
- we interpret \bar{a} as typical lifetime of cross links and adhesion and use $1/\bar{a}$ as a reference value for β , ζ , β_{adh} and ζ_{adh}
- $1/(\bar{a}L)$ is used for the cross-link density ρ and $\overline{\rho_{adh}}/\bar{a}$ for the adhesion density ρ_{adh}
- κ^B is used for the energy U and all its contributions
- finally the reference values $\kappa^B \backslash (\epsilon L)$, $\kappa^B L$, $\kappa^B \backslash (\epsilon \overline{\rho_{adh}} L)$ and $\kappa^B \backslash L$ for scaling κ^S , κ^T , κ^F and κ^M respectively

The main scaling assumption is that the dimensionless parameter

$$\epsilon := \frac{\bar{a}v_0}{L}$$

is small, i.e. that the typical lifetime of cross-links and adhesions is small compared to the typical time an actin molecule spends in a filament. However this is at least not always reasonable for adhesions. These can occasionally form large, long-living complexes, which would definitely not satisfy this assumption. We therefore exclude such complexes in our description. Physically our assumption means that cross-links and adhesions cause forces that are felt as friction by the

filaments.

Using the same symbols as for the unscaled quantities we get:

$$U_{bend}^\pm(t) [G^\pm] := \frac{1}{2} \int_B |\partial_s^2 G^\pm|^2 \eta^\pm d(\alpha, s) \quad (3.8)$$

$$U_{scl}(t) [G^+, G^-] := \frac{\kappa^S}{2\epsilon} \int_0^\infty \int_{\mathcal{C}(t-\epsilon a)} |S^\epsilon|^2 \rho^{eff} d(\alpha^+, \alpha^-) da$$

$$U_{tcl}(t) [G^+, G^-] := \frac{\kappa^T}{2} \int_0^\infty \int_{\mathcal{C}(t-\epsilon a)} (T^\epsilon)^2 \rho^{eff} d(\alpha^+, \alpha^-) da$$

$$U_{adh}^\pm(t) [G^\pm] := \frac{\kappa^F}{2\epsilon} \int_B \int_0^\infty |G^\pm - F^{\pm*}|^2 \rho_{adh}^\pm \eta^\pm d(\alpha, s) da \quad (3.9)$$

$$U_{memb} [G^\pm] := \kappa^M \left(\frac{C^+[G^+] + C^-[G^-]}{2} - C_0 \right)_+^2$$

with

$$\begin{aligned} S^\epsilon &= G^+(t, \alpha^+, s_{\epsilon a}^+(t, \alpha^+, \alpha^-)) - G^-(t, \alpha^-, s_{\epsilon a}^-(t, \alpha^+, \alpha^-)) \\ T^\epsilon &= \phi_{\epsilon a}(t, \alpha^+, \alpha^-) - \phi_0 \end{aligned} \quad (3.10)$$

and

$$F^{\pm*} := F^\pm \left(t - \epsilon a, \alpha^\pm, s + \int_{t-\epsilon a}^t v^\pm(\tilde{t}, \alpha), d\tilde{t} \right)$$

The PDEs for the cross-link and adhesion density become:

$$\begin{aligned} \epsilon \partial_t \rho + \partial_a \rho &= -\zeta(S, T) \rho \\ \rho(a=0) &= \beta(T_0) \left(1 - \int_0^\infty \rho da \right) \\ \rho(t, a, \alpha^+, \alpha^-) &= 0 \quad \text{for } (\alpha^+, \alpha^-) \in \mathcal{C}(t-\epsilon)_+ \\ \rho(t=0) &= \rho^I \end{aligned}$$

with T_0 defined as in (3.3).

$$\begin{aligned} \epsilon D_t^\pm \rho_{adh}^\pm + \partial_a \rho_{adh}^\pm &= -\zeta_{adh}(S_{adh}^\pm) \rho_{adh}^\pm \\ \rho_{adh}^\pm(a=0) &= \beta_{adh} \left(1 - \int_0^\infty \rho_{adh}^\pm da \right) \\ \rho_{adh}^\pm(s=0) &= 0 \\ \rho_{adh}^\pm(t=0) &= \rho_{adh}^{I\pm} \end{aligned}$$

with

$$\begin{aligned} S_{adh}^\pm(t, a, \alpha^\pm, s) &= F^\pm(t, \alpha^\pm, s) - F^\pm \left(t - \epsilon a, \alpha^\pm, s + \epsilon \int_{t-a}^t v^\pm(\tilde{t}) d\tilde{t} \right) \\ D_t^\pm &:= \partial_t - v^\pm \partial_s \quad \text{the material derivative} \end{aligned}$$

The solution of their corresponding limiting equations for $\epsilon \rightarrow 0$ reads:

$$\rho = \frac{\beta(T_0)\zeta(0, T_0)}{\beta(T_0) + \zeta(0, T_0)} e^{-\zeta(0, T_0)a}$$

$$\rho_{adh}^{\pm} = \frac{\beta_{adh}\zeta_{adh}(0)}{\beta_{adh} + \zeta_{adh}(0)} e^{-\zeta_{adh}(0)a}$$

Note that these are singular limits and that eventual boundary and initial layers were ignored. ρ depends on $T_0(t, \alpha^+, \alpha^-)$; this dependence is local in time.

To take $\epsilon \rightarrow 0$ in the energy contributions one needs to look at the corresponding variational problem. We define

$$\mathcal{I}(\tau) := U [F^+ + \tau\delta F^+, F^- + \tau\delta F^-]$$

Because U , the sum of all energy contributions, has a minimum at (F^+, F^-) , it has to be true that $\mathcal{I}'(\tau)|_{\tau=0} = 0$ for all admissible variations $(\delta F^+, \delta F^-)$, i.e.

$$\delta U [F^+, F^-] (\delta F^+, \delta F^-) = 0$$

To account for the constraints in (3.7) Lagrange multipliers are introduced which give the additional contributions:

$$U_{ext}^{\pm} [G^{\pm}] = \frac{1}{2} \int_B \lambda^{\pm}(\alpha, s) \left(|\partial_s G^{\pm}(\alpha, s)|^2 - a \right) \eta^{\pm} d(\alpha, s)$$

$$U_{edge} [G^+, G^-] = \int_{-\pi}^{\pi} \lambda_{edge}(\alpha^+) (G^+(t, \alpha^+, 0) - G^-(t, \hat{\alpha}(t, \alpha^+), 0)) \cdot \nu(t, \alpha^+) d\alpha^+$$

The first expression describes the inextensibility of filaments and the second the deviation between the outer edges of the two filament families. $\hat{\alpha}(t, \alpha^+)$ is chosen such that $G^+(t, \alpha^+, 0) - G^-(t, \hat{\alpha}(t, \alpha^+), 0)$ is parallel to $\nu(t, \alpha^+)$, which is the outward unit normal vector along the barbed ends of the clockwise filaments.

In a next step the variations of the contributions are calculated and finally ϵ is taken to zero. Without going into further detail one gets:

$$\begin{aligned} \delta U_{ext}^{\pm} [F^{\pm}] \delta F^{\pm} &= \int_B \lambda^{\pm} \partial_s F^{\pm} \cdot \partial_s \delta F^{\pm} \eta^{\pm} d(\alpha, s) & (3.11) \\ \delta U_{edge} [F^+, F^-] \delta F^{\pm} &= \pm \int_{-\pi}^{\pi} \lambda_{edge}^{\pm} \nu \cdot \delta F^{\pm}(s=0) d\alpha \\ \delta U_{memb} [F^{\pm}] \delta F^{\pm} &= \kappa^M (C^{\pm} - C_0)_+ \int_{-\pi}^{\pi} \frac{\partial_{\alpha} F^{\pm}(s=0)}{|\partial_{\alpha} F^{\pm}(s=0)|} \cdot \partial_{\alpha} \delta F^{\pm}(s=0) d\alpha \\ \delta U_{bend}^{\pm} [F^{\pm}] \delta F^{\pm} &= \int_B \partial_s^2 F^{\pm} \cdot \partial_s^2 \delta F^{\pm} \eta^{\pm} d(\alpha, s) \\ \delta U_{adh}^{\pm} [F^{\pm}] \delta F^{\pm} &= \mu^A \int_B D_t^{\pm} F^{\pm} \cdot \delta F^{\pm} \eta^{\pm} d(\alpha, s) \\ \delta U_{scl}(t) [F^+, F^-] \delta F^{\pm} &= \pm \int_{\mathcal{C}(t)} \mu^S(T_0) (D_t F^+ - D_t F^-) \delta F^{\pm} \eta^+ \eta^- d(\alpha^+, \alpha^-) \\ \delta U_{tcl}(t) [F^+, F^-] \delta F^{\pm} &= \mp \int_{\mathcal{C}(t)} \mu^T(T_0) T_0 (\partial_s F^{\pm\pm} \cdot \partial_s \delta F^{\pm}) \eta^+ \eta^- d(\alpha^+, \alpha^-) \end{aligned}$$

In $\delta U_{tcl}(t)$ $\partial_s F^\pm$ and $\partial_s \delta F^\pm$ are evaluated at $(t, \alpha^\pm, s^\pm(t, \alpha^+, \alpha^-))$. The following abbreviations were used:

$$\begin{aligned}\mu^S(T_0) &= \frac{\kappa^S \beta(T_0)}{\zeta(0, T_0) (\beta(T_0) + \zeta(0, T_0))} \\ \mu^T(T_0) &= \frac{\kappa^T \beta(T_0)}{\beta(T_0) + \zeta(0, T_0)} \\ \mu^A &= \frac{\kappa^A \beta_{adh}}{\zeta_{adh}(0) (\beta_{adh} + \zeta_{adh}(0))} \\ \lambda_{edge}^+ &= \lambda_{edge}(\alpha) \\ \lambda_{edge}^- &= \lambda_{edge}(\alpha^+(t, \alpha, 0))\end{aligned}$$

If the seven terms in (3.11) are collected one gets the following variational equation where there is no restriction on the variations δF^+ and δF^- .

$$\begin{aligned}& \int_{-\pi}^{\pi} \left[\kappa^M (C^\pm - C_0)_+ \frac{\partial_\alpha F^\pm(s=0)}{|\partial_\alpha F^\pm(s=0)|} \cdot \partial_\alpha \delta F^\pm \pm \lambda_{edge}^\pm \nu \cdot \delta F^\pm \right]_{s=0} d\alpha \\ & \pm \int_{\mathcal{C}(t)} (\mu^S(T_0) (D_t F^+ - D_t F^-) \delta F^\pm - \mu^T(T_0) T_0 (\partial_s F^{\pm\pm} \cdot \partial_s \delta F^\pm)) \eta^+ \eta^- d(\alpha^+, \alpha^-) \\ & + \int_B (\partial_s^2 F^\pm \cdot \partial_s^2 \delta F^\pm + \mu^A D_t^\pm F^\pm \cdot \delta F^\pm + \lambda^\pm \partial_s F^\pm \cdot \partial_s \delta F^\pm) \eta^\pm d(\alpha, s) = 0\end{aligned}$$

To derive an Euler-Lagrange equation the integration domains of the second and the third integral have to be mapped to each other via the transformation $(\alpha^+, \alpha^-) \mapsto (\alpha, s) = (\alpha^\pm, s^\pm(t, \alpha^+, \alpha^-))$. We incorporate the corresponding Jacobians and the fact that these terms only contribute in $B^\pm(t)$ into μ^S and μ^T via:

$$\mu_{\pm}^S := \begin{cases} \mu^S \left| \frac{\partial_\alpha^\mp}{\partial_s^\pm} \right| & \text{in } B^\pm(t) \\ 0 & \text{in } B \setminus B^\pm(t) \end{cases} \quad \mu_{\pm}^T := \begin{cases} \mu^T \left| \frac{\partial_\alpha^\mp}{\partial_s^\pm} \right| & \text{in } B^\pm(t) \\ 0 & \text{in } B \setminus B^\pm(t) \end{cases}$$

Finally we get the Euler-Lagrange equation:

$$\begin{aligned}& \overbrace{\partial_s^2 (\eta^\pm \partial_s^2 F^\pm)}^{\text{bending}} - \overbrace{\partial_s (\eta^\pm \lambda^\pm \partial_s F^\pm)}^{\text{inextensibility}} + \overbrace{\eta^\pm \mu^A D_t^\pm F^\pm}^{\text{adhesions}} \\ & \pm \underbrace{(\eta^+ \eta^- T_0 \mu_{\pm}^T(T_0) \partial_s F^{\pm\pm})}_{\text{twisting cross-links}} \pm \underbrace{\eta^+ \eta^- \mu_{\pm}^S(T_0) (D_t^+ F^+ - D_t^- F^-)}_{\text{stretching cross-links}} = 0\end{aligned} \quad (3.12)$$

Together with the boundary conditions:

$$\begin{aligned}\text{for } s = -L : \\ -\partial_s (\eta^\pm \partial_s^2 F^\pm) + \eta^\pm \lambda^\pm \partial_s F^\pm \mp \eta^+ \eta^- \mu_{\pm}^T(T_0) \partial_s F^{\pm\pm} = 0\end{aligned} \quad (3.13)$$

$$\begin{aligned}\text{for } s = 0 : \\ \partial_s (\eta^\pm \partial_s^2 F^\pm) - \lambda^\pm \partial_s F^\pm \pm \mu_{\pm}^T(T_0) \partial_s F^{\pm\pm} \\ = \pm \lambda_{edge}^\pm \nu - \kappa^M (C^\pm - C_0)_+ \partial_\alpha \left(\frac{\partial_\alpha F^\pm}{|\partial_\alpha F^\pm|} \right)\end{aligned} \quad (3.14)$$

$$\begin{aligned}\text{for } s = -L, 0 : \\ \eta^\pm \partial_s^2 F^\pm = 0\end{aligned}$$

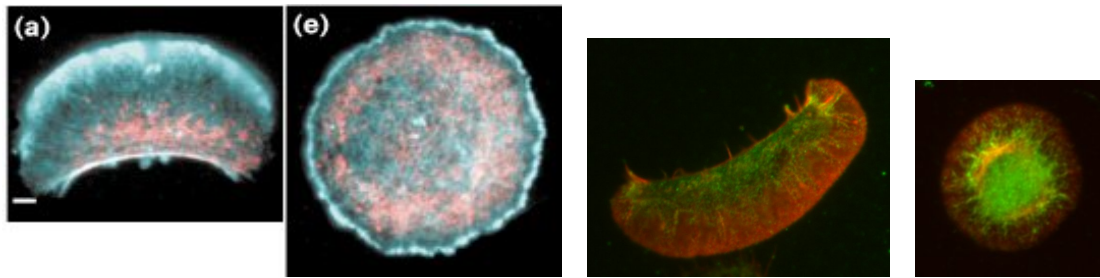


Figure 3.4: The left two pictures were taken by Verkhovsky et al. [1999], the right by myself. Both show the actin (cyan and red) and myosin (red and green) distribution in a moving and stationary cytoplast.

The Lagrange multipliers have to be determined such that the constraints (3.7) are fulfilled.

3.3 Introducing Myosin to the Model

3.3.1 Observations and Modeling

The basis of the modeling are observations taken from Verkhovsky et al. [1999] and my own experiments in the laboratory of Prof. Victor Small at the IMBA, Vienna (details in Chapter 1, Section 1.1 and in my bachelor's thesis). Figure 3.4 shows a moving and stationary cytoplast and the actin and myosin distributions. The two sets of pictures were produced by Verkhovsky et al. [1999] and myself and even though they do not show exactly the same distributions, they contain qualitatively the same information. Observations about the dynamics of myosin were all taken from Verkhovsky et al. [1999] and not reproduced.

For stationary cytoplasts

- Myosin spots start forming throughout most of the cytoplast but slightly away from the boundary.
- The spots move slowly towards the center and disappear.

For moving cytoplasts

- Myosin spots start forming near the front.
- They move inwards while growing bigger.
- They begin to form arc shaped bundles at the rear where they finally disassemble

Using the cross-link (CL) modeling as a starting point we now make the following assumptions about the myosin filaments (MF):

a) General remarks

- MF sit on two actin filaments, grow and exert a twisting and stretching force on the actin
- the twisting force is assumed to come from the stiffness of the (long) MF

b) The myosin filaments (MF) are modeled similar to cross-links, in particular:

- they connect actin filaments of the + and - family by attaching to actin monomers in the filaments
 - they can be created spontaneously at filament crossings
 - they can break
 - there cannot be more than one MF per crossing
 - their distribution is described by a density ρ_{myo}
- c) **Additional assumptions**
- CL and MF formation and breakage is independent from each other
 - the MF move towards the barbed ends of their actin filaments with speed v_{myo}
 - the preferred angle of a MF is π
 - MF grow with increasing age a and if the angles formed by the actin filaments is close to π
- d) **There are several consequences of a large size N of the MF:**
- the MF walk faster towards the barbed end, $v_{myo}(N)$
 - the twisting and stretching forces created by the MF grow, $\kappa^{SM}(N)$ and $\kappa^{TM}(N)$
 - the MF are less likely to break, $\zeta_{myo}(N)$

In summary we add the following assumption to **A1-A7**:

A8: *A myosin filament is a connection between material points on a clockwise and an anti-clockwise filament. Myosin filaments walk towards the barbed ends of both filaments with a certain velocity. Myosin filaments can be created spontaneously at the crossing between two filaments and they can also break. Creation and breaking are stochastic processes. There exists at most one myosin filament for any pair of filaments at any time. The formation of cross-links and myosin filaments is independent.*

3.3.2 Deriving Energy Contributions

Myosin filaments move along the actin monomers towards the barbed end of the actin filament, therefore the s-labels change in a way that depends on their velocity $v_{myo}(N(t, a, \alpha^+, \alpha^-))$, where the size of the MF, $N(t, a, \alpha^+, \alpha^-)$, is still to be specified (in the following we often omit arguments of N for simplicity).

$$s_{myo,a}^{\pm}(t, \alpha^+, \alpha^-) := s^{\pm}(t - a, \alpha^+, \alpha^-) - \int_{t-a}^t v^{\pm}(\tilde{t}, \alpha^{\pm}) - v_{myo}(N(\tilde{t}, \tilde{t} - (t - a), \alpha^+, \alpha^-)) d\tilde{t}$$

Note: The speed v_{myo} opposes the polymerization speed v^{\pm} , compare to (3.1).

Similar to (3.2) the stretching term S_{myo} stems from the distance between the actin monomers that the MF ends are attached to; the twisting term T_{myo} describes the deviation of the angle between the actin filaments from π :

$$\begin{aligned} S_{myo}(t, a, \alpha^+, \alpha^-) &:= F^+(t, \alpha^+, s_{myo,a}^+(t, \alpha^+, \alpha^-)) - F^-(t, \alpha^+, s_{myo,a}^-(t, \alpha^+, \alpha^-)) \\ T_{myo}(t, a, \alpha^+, \alpha^-) &:= \phi_{myo,a}(t, \alpha^+, \alpha^-) - \pi \\ \phi_{myo,a}(t, \alpha^+, \alpha^-) &:= \arccos[\partial_s F^+(t, \alpha^+, s_{myo,a}^+(t, \alpha^+, \alpha^-)) \cdot \partial_s F^-(t, \alpha^-, s_{myo,a}^-(t, \alpha^+, \alpha^-))] \end{aligned}$$

We see that $T_{myo}(t, 0, \alpha^+, \alpha^-) = T_0(t, \alpha^+, \alpha^-)$ (compare to (3.3)).

Remark: At this stage we have created a delay problem, because we would have to store information about the filament from time $t - a$ to time t . However, the problem will become local in time by scaling (see Section 3.3.4).

Analogously to the cross-link density (compare to (3.4)), we can write a transport equation for the MF density $\rho_{myo}(t, a, \alpha^+, \alpha^-)$:

$$\begin{aligned} \partial_t \rho_{myo} + \partial_a \rho_{myo} &= -\zeta_{myo}(S_{myo}, T_{myo}, N) \rho_{myo} \\ \rho_{myo}(a = 0) &= \beta_{myo}(T_0) \left(1 - \int_0^\infty \rho_{myo} d\tilde{a}\right) \end{aligned}$$

To get an effective MF density, ρ_{myo}^{eff} we need to take into account the length distributions of the actin filaments η^+ and η^- . By setting $\rho_{myo}^{eff} := \rho_{myo} \eta^+ \eta^-$, we again get a transport equation with adjusted breaking rate ζ_{myo}^{eff} :

$$\begin{aligned} \zeta_{myo}^{eff} &:= \zeta_{myo}(S_{myo}, T_{myo}, N) - \frac{\partial_t \eta^+ - (v^+ - v_{myo}(N)) \partial_s \eta^+}{\eta^+} - \frac{\partial_t \eta^- - (v^- - v_{myo}(N)) \partial_s \eta^-}{\eta^-} \\ \partial_t \rho_{myo}^{eff} + \partial_a \rho_{myo}^{eff} &= -\rho_{myo}^{eff} \zeta_{myo}^{eff} \end{aligned}$$

Now the forces stemming from stretching and twisting the myosin filaments are added to the other forces acting on the actin filaments described in (3.6).

$$\begin{aligned} U_{smyo}[G^+, G^-](t) &:= \int_0^\infty \int_{\mathcal{C}(t-a)} \left(\frac{\kappa^{SM}}{2} |S_{myo}|^2 \right) \rho_{myo}^{eff} d(\alpha^+, \alpha^-) da \\ U_{tmyo}[G^+, G^-](t) &:= \int_0^\infty \int_{\mathcal{C}(t-a)} \left(\frac{\kappa^{TM}}{2} T_{myo}^2 \right) \rho_{myo}^{eff} d(\alpha^+, \alpha^-) da \end{aligned}$$

Where $\mathcal{C}(t - a)$ describes the set of index pairs (α^+, α^-) which had a crossing point at time $t - a$.

Remark: Even though they look similar to the corresponding cross-link terms, note that κ^{SM} and κ^{TM} depend on the size N and also S_{myo} and T_{myo} via $s_{myo,a}^\pm$ as well as ρ_{myo}^{eff} .

3.3.3 Non-dimensionalization and Scaling the Energy Contributions

Discussion: One important assumption on the myosin filaments, is that their lifetime in the moving cytoplasts is much longer than in the stationary ones. We assume that in the stationary ones the forming and breaking happens much more often, consequently the lifetime of a MF is shorter than in the moving cytoplasts.

This brings up the question of the right choice of reference lifetime a_{myo}^{ref} . Two possible choices would be:

- a) $a_{myo}^{ref} = \bar{a} = \frac{\epsilon L}{v_0}$: This models an average MF lifetime which is short and similar to the lifetime of a cross-link and might be appropriate for stationary cytoplasts.
- b) $a_{myo}^{ref} = \frac{L}{v_0}$: This assumes an average lifetime similar to the time a monomer spends inside a filaments and seems reasonable for moving cytoplasts.

As our simulation goal at this point is destabilizing the stationary cytoplast to become a moving one, we will take the stationary one as a starting point and choose option a). However one has to keep on mind that on the long run, a change in scaling or other approach might be necessary.

All other variables are scaled analogously to before with choosing the reference values for κ^{SM} and κ^{TM} to be $\kappa^B/(\epsilon L)$ and $\kappa^B L$ respectively.

Myosin-Filament Density

The equations for ρ_{myo} now take the following form:

$$\begin{aligned} \epsilon \partial_t \rho_{myo} + \partial_a \rho_{myo} &= -\zeta_{myo}(S_{myo}^\epsilon, T_{myo}^\epsilon, N) \rho_{myo} \\ \rho_{myo}(a=0) &= \beta_{myo}(T_0) \left(1 - \int_0^\infty \rho_{myo} da\right) \\ \rho_{myo}(t, a, \alpha^+, \alpha^-) &= 0 \text{ for } (\alpha^+, \alpha^-) \in \partial\mathcal{C}(t - \epsilon a)_+ \\ \rho_{myo}(t=0) &= \rho_{myo}^I \end{aligned} \quad (3.15)$$

with

$$\begin{aligned} S_{myo}^\epsilon &= G^+(t, \alpha^+, s_{myo,a}^{\epsilon+}) - G^-(t, \alpha^-, s_{myo,a}^{\epsilon-}) \\ T_{myo}^\epsilon &= \phi_a^\epsilon(t, \alpha^+, \alpha^-) - \pi \\ \phi_a^\epsilon &= \arccos[\partial_s G^+(t, \alpha^+, s_{myo,a}^{\epsilon+}(t, \alpha^+, \alpha^-)) \cdot \partial_s G^-(t, \alpha^-, s_{myo,a}^{\epsilon-}(t, \alpha^+, \alpha^-))] \\ s_{myo,a}^{\epsilon\pm}(t) &:= s^\pm(t - \epsilon a, \alpha^+, \alpha^-) - \int_{t-\epsilon a}^t v^\pm(\tilde{t}, \alpha^\pm) - v_{myo}(N(\tilde{t}, \frac{\tilde{t}-t}{\epsilon} + a, \alpha^+, \alpha^-)) d\tilde{t} \end{aligned} \quad (3.16)$$

It is easy to see that $s_{myo,a}^{\epsilon\pm} \rightarrow s^\pm(t, \alpha^+, \alpha^-)$ and therefore $S_{myo}^\epsilon \rightarrow 0$ and $T_{myo}^\epsilon \rightarrow T_0$ as $\epsilon \rightarrow 0$.

We need to specify the dependence of ρ_{myo} on the size of a myosin filament, N . A myosin filament grows if more myosin monomers attach to it (for more details see Chapter 1). Therefore more heads can act on actin leading to an increase in forces and moving speed. We expect the myosin's growth to depend on how favorable the angle between its actin filaments is:

$$\partial_a N(t, a, \alpha^+, \alpha^-) = R(\phi(t + a, \alpha^+, \alpha^-)), \quad N(t, 0, \alpha^+, \alpha^-) = 0$$

Where a is the age of the MF and R is an increasing function of ϕ which takes its minimum at $\phi = 0$ (parallel actin filaments) and its maximum at $\phi = \pi$ (anti-parallel filaments). Using the same scaling as before and choosing as a reference value for R , $R^{ref} = \frac{L}{a}$, we get:

$$\partial_a N(t, a, \alpha^+, \alpha^-) = R(\phi(t + \epsilon a, \alpha^+, \alpha^-)), \quad N(t, 0, \alpha^+, \alpha^-) = 0$$

So with $\epsilon \rightarrow 0$

$$N(t, a, \alpha^+, \alpha^-) = a R(\phi(t, \alpha^+, \alpha^-))$$

With this we can calculate the myosin filament density ρ_{myo} . We set $N(t, a, \alpha^+, \alpha^-) = a R(\phi(t, \alpha^+, \alpha^-))$ in (3.15) and thereby change from $\rho_{myo}(t, a, \alpha^+, \alpha^-)$ to $\rho_{myo}(t, N, \alpha^+, \alpha^-)$. The new equations (after taking $\epsilon \rightarrow 0$) read:

$$\begin{aligned} R(\phi) \partial_N \rho_{myo} &= -\zeta_{myo}(0, T_0, N) \rho_{myo} \\ \rho_{myo}(N=0) &= \beta_{myo}(T_0) \left(1 - \frac{1}{R(\phi)} \int_0^\infty \rho_{myo} d\tilde{N}\right) \end{aligned}$$

The solution of the PDE takes the following form :

$$\begin{aligned} \rho_{myo}(t, N) &= \rho_{myo}(t, 0) \exp\left(-\frac{1}{R(\phi(t))} \int_0^N \zeta_{myo}(0, T_0(t), \tilde{N}) d\tilde{N}\right) \\ \rho_{myo}(t, 0) &= \frac{\beta(T_0)}{1 + \frac{\beta(T_0(t))}{R(\phi(t))} \int_0^\infty \left(\exp\left(-\frac{1}{R(\phi(t))} \int_0^N \zeta_{myo}(0, T_0(t), \tilde{N}) d\tilde{N}\right)\right) dN} \end{aligned} \quad (3.17)$$

For better readability we omitted the arguments α^+ and α^- , but note that we have: $\phi(t, \alpha^+, \alpha^-)$ and $T_0(t, \alpha^+, \alpha^-)$ and therefore $\rho_{myo}(t, N, \alpha^+, \alpha^-)$.

Energy Contributions

The energy contributions that are to be added to the list in (3.8) become:

$$\begin{aligned} U_{smyo}[G^+, G^-](t) &:= \frac{1}{\epsilon} \int_0^\infty \int_{\mathcal{C}(t-\epsilon a)} \left(\frac{\kappa^{SM}}{2} |S_{myo}^\epsilon|^2\right) \rho_{myo}^{eff} d(\alpha^+, \alpha^-) da \\ U_{tmyo}[G^+, G^-](t) &:= \int_0^\infty \int_{\mathcal{C}(t-\epsilon a)} \left(\frac{\kappa^{TM}}{2} (T_{myo}^\epsilon)^2\right) \rho_{myo}^{eff} d(\alpha^+, \alpha^-) da \end{aligned}$$

with the abbreviations as defined in (3.16).

To understand what happens with the energy contributions for $\epsilon \rightarrow 0$ we again need to look at the variational problem.

We start with the stretching term and calculate its variation to be:

$$\delta U_{smyo}(t) [F^+, F^-] \delta F^\pm = \pm \frac{1}{\epsilon} \int_0^\infty \int_{\mathcal{C}(t-\epsilon a)} \kappa^{SM} S_{myo}^\epsilon \delta F^\pm(t, \alpha^\pm, s_{myo,a}^{\epsilon,\pm}) \rho_{myo}^{eff} d(\alpha^+, \alpha^-) da$$

To be able to take the limit we need to examine S_{myo}^ϵ further (for simplicity we will omit all α^+ and α^-):

$$\begin{aligned} S_{myo}^\epsilon &= \underbrace{(F^+(t, s(t-\epsilon a)) - F^+(t-\epsilon a, s(t-\epsilon a)))}_A \\ &\quad - \underbrace{\left(F^+(t, s(t-\epsilon a)) - F^+\left(t, s(t-\epsilon a) - \int_{t-\epsilon a}^t v^+(\tilde{t}) - v_{myo}\left(N\left(\tilde{t}, \frac{1}{\epsilon}(\tilde{t}-t) + a\right)\right) d\tilde{t}\right)}_B \\ &\quad - \left[(F^-(t, s(t-\epsilon a)) - F^-(t-\epsilon a, s(t-\epsilon a))) \right. \\ &\quad \left. - \left(F^-(t, s(t-\epsilon a)) - F^-\left(t, s(t-\epsilon a) - \int_{t-\epsilon a}^t v^-(\tilde{t}) - v_{myo}\left(N\left(\tilde{t}, \frac{1}{\epsilon}(\tilde{t}-t) + a\right)\right) d\tilde{t}\right)\right) \right] \end{aligned} \quad (3.18)$$

Now we will look only at the F^+ case in (3.18). The two brackets appearing we call A and B . Using a first order Taylor expansion in the first variable, i.e. $F^+(t-\epsilon a, s) = F^+(t, s) - \partial_t F^+(t, s)\epsilon a + \mathcal{O}(\epsilon^2)$, we see that:

$$A = \epsilon a \partial_t F^+(t, s(t-\epsilon a)) + \mathcal{O}(\epsilon^2)$$

Part B requires some more work. First we take care of the integrals: The first one we Taylor

expand:

$$\int_{t-\epsilon a}^t v^+(\tilde{t}) d\tilde{t} = \epsilon a v^+(t) + \mathcal{O}(\epsilon^2) \quad (3.19)$$

In the second integral we perform a change of variables $\tilde{a} = \frac{\tilde{t}-t}{\epsilon} + a$ and then do a Taylor expansion of the integrand, receiving:

$$\begin{aligned} \int_{t-\epsilon a}^t v_{myo} \left(N \left(\tilde{t}, \frac{1}{\epsilon}(\tilde{t}-t) + a \right) \right) d\tilde{t} & \quad (3.20) \\ &= \epsilon \int_0^a v_{myo} (N((\tilde{a}-a)\epsilon + t, \tilde{a})) d\tilde{a} \\ &= \epsilon \int_0^a v_{myo} (N(t, \tilde{a})) d\tilde{a} + \epsilon \int_0^a \partial_t v_{myo} (N(t, \tilde{a})) \epsilon(\tilde{a}-a) d\tilde{a} + \mathcal{O}(\epsilon^2) \\ &= \epsilon \int_0^a v_{myo} (N(t, \tilde{a})) d\tilde{a} + \mathcal{O}(\epsilon^2) \end{aligned}$$

Now we Taylor expand B in the second variable and using the integrals in (3.19) and (3.20) we get:

$$B = \epsilon a \left(v^+(t) - \frac{1}{a} \int_0^a v_{myo} (N(t, \tilde{a})) d\tilde{a} \right) \partial_s F(t, s(t-\epsilon a)) + \mathcal{O}(\epsilon^2) \quad (3.21)$$

Now we do the same for the $-$ family and, putting everything together and letting $\epsilon \rightarrow 0$, we get:

$$\delta U_{smyo}(t) [F^+, F^-] \delta F^\pm = \pm \int_0^\infty \int_{\mathcal{C}(t)} \kappa^{SM} a (D_{t,a}^+ F^+ - D_{t,a}^- F^-) \delta F^\pm \rho_{myo} \eta^+ \eta^- d(\alpha^+, \alpha^-) da \quad (3.22)$$

$$D_{t,a}^\pm F^\pm := \partial_t F^\pm - \left(v^\pm(t) - \frac{1}{a} \int_0^a v_{myo} (N(t, \tilde{a})) d\tilde{a} \right) \partial_s F^\pm$$

$D_{t,a}^\pm$ looks similar to a material derivative, but accounts for the (forward) movement of MFs which opposes the backwards movement of actin monomers caused by polymerisation. This also explains the minus between the two velocity terms. Furthermore does the expression $\frac{1}{a} \int_0^a v_{myo} d\tilde{a}$ represent an average of v_{myo} over different ages, which seems reasonable.

For the twisting term we proceed analogously to the twisting of the cross-links and get:

$$\delta U_{tmyo}(t) [F^+, F^-] \delta F^\pm = \mp \int_0^\infty \int_{\mathcal{C}(t)} \kappa^{TM} T_0 (\partial_s F^{\pm\pm} \cdot \partial_s \delta F^\pm) \rho_{myo} \eta^+ \eta^- d(\alpha^+, \alpha^-) da \quad (3.23)$$

Please note that κ^{SM} , κ^{TM} , v_{myo} and ρ_{myo} all depend on the size of the MF N . In order to proceed we need to specify those dependencies.

3.3.4 Modeling the Dependencies on the Size of a Myosin Filament

From (3.22) and (3.23) we see that to find the corresponding Euler-Lagrange terms we need to calculate the following integrals:

$$I_1 := \int_0^\infty \kappa^{SM}(a) a \rho_{myo}(a) da = \frac{1}{R^2} \int_0^\infty \kappa^{SM}(N) N \rho_{myo}(N) dN \quad (3.24)$$

$$I_2 := \int_0^\infty \kappa^{SM}(a) a \rho_{myo}(a) \frac{1}{a} \int_0^a v_{myo}(\tilde{a}) d\tilde{a} da = \frac{1}{R^2} \int_0^\infty \kappa^{SM}(N) \rho_{myo}(N) \int_0^N v_{myo}(\tilde{N}) d\tilde{N}$$

$$I_3 := \int_0^\infty \kappa^{TM}(a) \rho_{myo}(a) da = \frac{1}{R} \int_0^\infty \kappa^{TM}(N) \rho_{myo}(N) dN$$

The question is which dependencies are necessary to produce a destabilizing effect in the stationary cytoplasm. What we want to create is a positive feedback loop that, if a large enough asymmetry in the circular cytoplasm occurs, can reinforce it and produce a polarized fragment. In a first attempt we try varying only one of the parameters, that is either

- a) the velocity of the myosin filament bundle v_{myo} or
- b) the Hook constants κ^{SM} and κ^{TM} or
- c) the breaking rate ζ_{myo} of myosin filaments

For simplicity we omit all arguments except N in the following.

We start with option a

In Chapter 2 we saw in (2.9) a dependence of the bundle speed (there called u) on the size N of the form $v_{myo} = C_1 \left(1 - \frac{C_2}{N}\right)$ for some constants C_1 and C_2 . For the lamellipodium we want 0 speed for 0 size and otherwise positive speed and write $v_{myo}(N) := \bar{v} \left(1 - \frac{b}{N+b}\right)$ for some constant $b > 0$ and maximum speed \bar{v} .

Remark: To be precise the dependence in Chapter 2 had the form $v_{myo} = C_1 \left(1 - \frac{F C_2}{N}\right)$ for an external force F . In our case this would be the stretching force S described above. This would result in a much more complicated dependence, but should be analyzed separately. Here we will work with the simplified version.

For the myosin filament density ρ_{myo} we assume $\zeta_{myo}(N) \equiv \bar{\zeta}$ and get

$$\rho_{myo}(N) = \rho_{myo}(0) e^{-\frac{\bar{\zeta}}{R} N}$$

$$\rho_{myo}(0) = \frac{\beta(T_0) \bar{\zeta}}{\bar{\zeta} + \beta(T_0)}$$

Further we assume $\kappa^{SM}(N) \equiv \bar{\kappa}^S$ and likewise $\kappa^{TM}(N) \equiv \bar{\kappa}^T$. With these assumptions we get for the integrals in (3.24):

$$I_1 = \frac{\bar{\kappa}^S \rho_{myo}(0)}{\bar{\zeta}^2} =: \mu^{SM}(T_0)$$

$$I_2 = \mu^{SM} \bar{v} f(R)$$

$$I_3 = \frac{\bar{\kappa}^T \rho_{myo}(0)}{\bar{\zeta}} =: \mu^{TM}(T_0)$$

Where $f(R) = \left(1 - \frac{b\bar{\zeta}}{R} \exp\left(\frac{b\bar{\zeta}}{R}\right) Ei\left(1, \frac{b\bar{\zeta}}{R}\right)\right)$. Here $Ei(1, \gamma)$ with $\gamma > 0$ calls the "Exponential Integral" defined by $\int_1^\infty e^{-\gamma s} s^{-1} ds$. $f(R) \sim 1$ for large R .

In the variational equation we therefore get the following contributions:

$$\pm \int_{\mathcal{C}(t)} \mu^{SM}(T_0) \left(\tilde{D}_{t,R}^+ F^+ - \tilde{D}_{t,R}^- F^- \right) \delta F^\pm \eta^+ \eta^- d(\alpha^+, \alpha^-)$$

$$\mp \int_{\mathcal{C}(t)} \mu^{TM}(T_0) T_0 \partial_s F^{\pm\perp} \cdot \partial_s \delta F^\pm \eta^+ \eta^- d(\alpha^+, \alpha^-)$$

$$\tilde{D}_{t,R}^\pm F^\pm := \partial_t F^\pm - (v^\pm - \tilde{v}f(R)) \partial_s F^\pm$$

and finally by defining

$$\mu_\pm^{SM} = \begin{cases} \mu^{SM} \left| \frac{\partial \alpha^\mp}{\partial s^\mp} \right| & \text{in } B^\pm(t) \\ 0 & \text{in } B \setminus B^\pm(t) \end{cases}$$

$$\mu_\pm^{TM} = \begin{cases} \mu^{TM} \left| \frac{\partial \alpha^\mp}{\partial s^\mp} \right| & \text{in } B^\pm(t) \\ 0 & \text{in } B \setminus B^\pm(t) \end{cases}$$

we get in the Euler-Lagrange equation in (3.12) the additional terms:

$$\pm \eta^+ \eta^- \mu_\pm^{SM}(T_0) \left(\tilde{D}_{t,R}^+ F^+ - \tilde{D}_{t,R}^- F^- \right)$$

$$\pm \partial_s (\eta^+ \eta^- T_0 \mu_\pm^{TM}(T_0) \partial_s F^{\pm\perp})$$

The main difference to the cross-links is the stretching term which has a modified material derivative. Lastly we also get additional terms in the boundary conditions, i.e. the term $\pm \eta^+ \eta^- \mu_\pm^{TM}(T_0) \partial_s F^{\pm\perp}$ in (3.13) and on the left side of (3.14).

Next we look at option b

Here we define $v_{myo}(N) \equiv \bar{v}$ and again $\zeta_{myo}(N) \equiv \bar{\zeta}$ resulting in the same ρ_{myo} as above. The Hook constants we model as follows:

$$\kappa^{SM}(N) := \bar{\kappa}^S (1 - e^{-h_s N})$$

$$\kappa^{TM}(N) := \bar{\kappa}^T (1 - e^{-h_t N})$$

We then get for the integrals in (3.24)

$$I_1 = \bar{\kappa}^S \rho_{myo}(0) \left(\frac{1}{\bar{\zeta}^2} - \frac{1}{(\bar{\zeta} + R h_s)^2} \right) =: \mu^{SM}(T_0)$$

$$I_2 = \bar{v} \mu^{SM}(T_0)$$

$$I_3 = \frac{\rho_{myo}(0) \bar{\kappa}^T}{\bar{\zeta}} \frac{R h_t}{R h_t + \bar{\zeta}} =: \mu^{TM}(T_0)$$

then we proceed as in case a.

Finally we examine option c

We expect the breaking rate $\zeta_{myo}(N)$ to decrease with increasing size. In order to ensure integrability of the terms in (3.17) and (3.24) we have to make sure the breaking rate doesn't decrease too fast. To that end we assume that the angle dependent growth rate $R(\phi)$ in $N = a R(\phi)$ is bounded and model $\zeta_{myo}(N) = \frac{a}{N+a} \bar{\zeta}$ with a large enough such that $\frac{\bar{\zeta} a}{R} > 2$ for all possible values of the (bounded) R .

If we now calculate $\rho_{myo}(N)$ according to (3.17) we get:

$$\rho_{myo}(N) = \rho_{myo}(0) a \frac{\bar{\zeta} a}{R} (N + a)^{\frac{\bar{\zeta} a}{R}}$$

$$\rho_{myo}(0) = \frac{\beta(T_0)}{1 + \frac{\beta(T_0)a}{a\bar{\zeta} - R}}$$

We set $\kappa^{SM}(N) \equiv \overline{\kappa^S}$, $\kappa^{TM}(N) \equiv \overline{\kappa^T}$ and $v_{myo}(N) \equiv \bar{v}$ and calculate the integrals:

$$I_1 = \overline{\kappa^S} \rho_{myo}(0) \frac{a^2}{(a\bar{\zeta} - R)(a\bar{\zeta} - 2R)} =: \mu^{SM}(T_0)$$

$$I_2 = \bar{v} \mu^{SM}(T_0)$$

$$I_3 = \overline{\kappa^T} \rho_{myo}(0) \frac{a}{a\bar{\zeta} - R} =: \mu^{TM}(T_0)$$

Now we can proceed as in case a.

3.4 Outlook

The next task is to implement these terms into an already existing Matlab code. It will be necessary to estimate parameters and if suitable to simplify the above expressions. The hoped for effect would be that

- a) if the program starts with a stationary cytoplasm, the myosin term should not disturb the state.
- b) if the stationary state is asymmetrically disturbed, the myosin terms should further reinforce the asymmetry, start making one side thinner with more anti-parallel actin filaments and therefore indicate a transition to the moving state.

If the cytoplasm simulation behaves in this way, it could be concluded that myosin has the power to cause the transition and further experimental proof and examination should be sought.

This work, however, is still in progress and not yet finished. Additionally different modeling in the cases a, b and c above could be done and/or a combination of the cases attempted.

Bibliography

- B. Alberts, A. Johnson, J. Lewis, M. Raff, K. Roberts, and P. Walter. *Molecular Biology of the Cell*, volume 4. Taylor and Francis, 2002.
- J. M. Berg, J. L. Tymoczko, and L. Stryer. *Biochemie*, volume 5. Spektrum Akademischer Verlag Heidelberg, 2003.
- L. Cramer. Forming the cell rear first: breaking cell symmetry to trigger directed cell migration. *Nature Cell Biology*, **12**:628–632, 2010.
- L. Evans. *Partial Differential Equations*, volume 19. American Mathematical Society, 1998.
- A. Huxley. Muscle structure and theories of contraction. *Progress in biophysics and biological chemistry*, **7**:255–318, 1957.
- D. Oelz and C. Schmeiser. Simulation of lamellipodial fragments. 2010a.
- D. Oelz and C. Schmeiser. Derivation of a Model for Symmetric Lamellipodia with Instantaneous Cross-Link Turnover. *Archive for Rational Mechanics and Analysis*, **198**:963–980, 2010b.
- D. Oelz and C. Schmeiser. *Cell Mechanics: From Single Scale-Based Models to Multiscale Modeling*, chapter How do Cells Move? A Mathematical Modeling of Cytoskeleton Dynamics and Cell Migration. Chapman and Hall, 2010c.
- D. Oelz, C. Schmeiser, and J. Small. Modeling of the actin-cytoskeleton in symmetric lamellipodial fragments. *Cell Adhesion and Migration*, **2**:117–126, 2008.
- H. Qian. The mathematical theory of molecular motor movement and chemomechanical energy transduction. *Journal of Mathematical Chemistry*, **27**:219–234, 2000.
- G. Teschl. *Ordinary Differential Equations and Dynamical Systems, to appear*. American Mathematical Society.
- A. Verkhovskiy, T. Svitkina, and G. Borisy. Myosin II Filament Assemblies in the Active Lamella of Fibroblasts: Their Morphogenesis and Role in the Formation of Actin Filament Bundles. *The Journal of Cell Biology*, **131**:989–1002, 1995.
- A. Verkhovskiy, T. Svitkina, and G. Borisy. Self-Polarisation and directional motility of cytoplasm. *Current Biology*, **9**:11–20, 1999.
- C. Wilson, M. Tsuchida, G. Allen, E. Barnhart, K. Applegate, P. Yam, L. Ji, K. Keren, G. Danuser, and J. Theriot. Myosin II contributes to cell-scale actin network treadmilling through network disassembly. *Nature*, **465**:373–377, 2010.
- P. Yam, C. Wilson, L. Ji, B. Herbert, E. Barnhart, N. Dye, P. Wiseman, G. Danuser, and J. Theriot. Actin-Myosin network reorganisation breaks symmetry at the cell rear to spontaneously initiate polarized cell motility. *The Journal of Cell Biology*, **178**:1207–1221, 2007.

Curriculum Vitae

Personal data

Name Angelika Manhart
Date of Birth 23rd of April, 1986
Place of Birth Vienna, Austria
Citizenship Austria

Schooling

1992-1996 Primary School Prückelmayergasse, Vienna
1996-2000 BRG 12 Singrienergasse, Vienna
2000-2002 Bilingual Highschool, Draschestraße, Vienna
2002-2003 Students Exchange to Nambour, Australia, Sunshine Coast Grammar School
2003-2004 Continuation of the Bilingual Highschool, Vienna
18th of June 2004 Matura passed with distinction

University

since 2004 Diploma Studies Mathematics, University of Vienna
since 2005 Diploma Studies Molecular Biology, University of Vienna
12th of Jan. 2007 1st diploma examination Mathematics passed with distinction
30th of Sept. 2010 1st diploma examination Molecular Biology passed with distinction

Additional Experiences and Scholarships

Summer 2005 Conductance of Mathematics Intensive Course at Lernquadrat, Vienna
2006 Performance Scholarship, University of Vienna
2007 Performance Scholarship, University of Vienna
2006-2008 Research Scholarship at the Department for Clinical Microbiology at the AKH, Vienna
2008 Voluntary social year in Uganda
Summer 2009 Work at the Department for Genetic Epidemiology, Medical University, Innsbruck
Summer 2009 MathMods summer school in Alba Adriatica, Italy
Autumn 2010 Work at the Myko Congress of the ÖGMM, Vienna
2010 Performance Scholarship, University of Vienna
Summer 2011 Tutor for the lecture "Mathematik für Molekularbiologen"

Foreign Languages

Italian: Basic knowledge, English: Excellent knowledge

Computer Experiences

Office Package, Matlab, Maple, Latex and Visual Basic